Cretaceous to Miocene cooling of Austroalpine units southeast of the Tauern Window (Eastern Alps) constrained by multi-system thermochronometry

Andreas WÖLFLER[1)*)], Christian DEKANT[2)], Wolfgang FRISCH[2)], Martin DANIŠÍK[3)] & Wolfgang FRANK[4)]

[1)] Institut für Geologie, Leibniz Universität Hannover, Callinstraße 30, D-30167 Hannover, Germany;

[2)] Institut für Geowissenschaften, Wilhelmstraße 56, D-72074 Tübingen, Germany;

[3)] Department of Earth & Ocean Sciences, Faculty of Science & Engineering, The University of Waikato, Hillcrest Road, Hamilton 3240, New Zealand;

[4)] Geological Institute, Slovak Academy of Sciences, Dúbravská cesta 9, SK-84005, Bratislava 45, Slovak Republic;

[*)] Corresponding author, woelfler@geowi.uni-hannover.de

DOI: 10.17738/ajes.2015.0002

KEYWORDS

thermal history modelling
fission track dating
geochronology
Eastern Alps

Abstract

The cooling history of the Polinik and Kreuzeck Blocks of the Austroalpine units to the southeast of the Tauern Window are re-examined in the light of new mica Ar/Ar-, zircon fission track and apatite fission track data. Our new data demonstrate that the two blocks experienced a significantly different thermal evolution during Mesozoic-Cenozoic times: The Polinik Block revealed Late Cretaceous Ar/Ar ages (87.2–81.6 Ma), which reflect cooling subsequent to the thermal peak of Eo-Alpine metamorphism. The Kreuzeck Block, in contrast, shows early Permian Ar/Ar ages (295–288 Ma) that reflect post-Variscan extension and cooling. Late Cretaceous zircon fission track ages (67.8 and 67.3 Ma) found in the Kreuzeck Block are interpreted to reflect post-metamorphic exhumational cooling after the Eo-Alpine metamorphism. Miocene apatite fission track ages (21.3–8.7 Ma) and transdimensional inverse thermal history modelling results suggest that the Polinik Block cooled rapidly through the apatite partial annealing zone and exhumed to near surface temperatures in the middle Miocene. The Kreuzeck Block, in contrast, cooled and exhumed to near surface temperatures already in the Oligocene and early Miocene as evidenced by apatite fission track ages (29.1–16.4 Ma) and thermal history modelling results. Based on the temperature difference between the uppermost and lowermost samples from steep elevation profiles, calculated paleo-geothermal gradients are in the range between 47 and 43 °C/km for the late Oligocene and middle Miocene periods. These high values likely resulted from an elevated heat flow associated with magmatism in the area and from the fast exhumation of hot Penninic domains during Oligocene and Miocene times.

Wir präsentieren neue Ar/Ar, Zirkon- und Apatitspaltspuralter vom ostalpinen Kristallin südöstlich des Tauernfensters. Die unterschiedlichen Altersverteilungen lassen auf verschiedene Abkühlphasen sowohl in mesozoischer als auch in känozoischer Zeit schließen. Der nördlich gelegene Polinik Block zeigt kretazische Ar/Ar Alter (87–81 Ma), welche als Abkühlalter unmittelbar nach dem Höhepunkt der eoalpinen Metamorphose interpretiert werden. Ar/Ar Daten aus dem südlich gelegenen Kreuzeck Block zeigen permische Alter (295–288 Ma). Das bedeutet, dass die eoalpine Deformation und Metamorphose nicht ausreichte, um diese Alter zurückzustellen. Mittels eines neuen Modellieransatzes können wir zeigen, dass sowohl der Kreuzeck- als auch der Polinik Block zu unterschiedlichen Zeiten zu oberflächennahen Temperaturen abkühlten. Demnach erreicht der Kreuzeck Block die partielle Ausheilzone von Apatitspaltspuren, zwischen 120 und 60 °C, bereits im Oligozän und frühen Miozän. Im Gegensatz dazu erreichte der Polinik Block diese Temperaturzone erst im mittleren Miozän. Aufgrund der Temperaturdifferenz zwischen den topographisch höchst- und tiefstgelegenen Proben von Höhenprofilen ist es uns möglich, den geothermischen Gradienten für das Oligozän und mittlere Miozän zu errechnen. Es zeigt sich, dass in dem genannten Zeitraum der geothermische Gradient zwichen 47 und 43 °C/km lag. Diese hohen Werte lassen sich mit magmatischen Aktivitäten entlang des Periadriatischen Störungssystems, beziehungsweise mit erhöhtem Wärmefluss durch die Exhumation von warmen penninischen Einheiten in Verbindung bringen.

1. Introduction

Geochronology has played an enormous role in unravelling of the complex history of the Eastern Alps. Since the pioneering studies in the 60´s and 70´s of the last century, the Alps have been extensively sampled for geochronological analyses which mostly involved muscovite and biotite for Rb/Sr, K/Ar and Ar/Ar dating methods, covering the temperature ranges of lower to middle crust (e.g. Oxburgh et al. 1966; Brewer and Jenkins, 1969; Lambert, 1970; Wagner et al., 1977; Thöni, 1999). With the advance of low-temperature thermochronology since the late 80´s, a growing number of zircon and apatite fission track data (ZFT and AFT, respectively) helped to resolve processes in the deeper levels of the upper crust (e.g. Wagner et al., 1977; Grundmann and Morteani, 1985; Staufenberg, 1987; Hejl, 1997, 1998; Dunkl et al., 2003; Foeken et al., 2007; Wölfler et al., 2008, 2012). And finally, the (U-Th)/He methods available since the beginning of this century allowed scientists to track shallow crystal processes operating at temperatures <100C° in the shallowest levels of the upper crust (e.g. Foeken et al., 2007; Glotzbach et al., 2008; Wölfler et al., 2008, 2012). One of the major challenges in geochronology is the proper reconstruction of thermal histories from measured data. The long accepted closure tempe-

rature concept (Dodson, 1973) is sound and viable in many cases, however, increased understanding of track annealing and diffusion kinetics in apatite and zircon (e.g. Fleischer et al., 1964, 1965, 1975; Wagner, 1968; Green et al., 1986; Carlson, 1990; Ketcham et al., 1999; Wendt et al., 2002; Farley, 2000; 2002; Meesters and Dunai, 2002; Reiners et al., 2003, 2004; Barbarand et al., 2003; Flowers et al., 2007; Guenthner et al., 2013) and development of user-friendly modelling packages that invert measured thermochronological data into cooling trajectories, provide scientists with much more robust tools for quantitative reconstruction of thermal histories of rocks (e.g. Gallagher, 1995, 2012; Gallagher et al., 2005, 2009; Ketcham, 2005; Ketcham et al., 2000; Meesters and Dunai, 2002). For high topography regions, such as the Eastern Alps, however, the 'classic' altitude dependence method (Wagner and Reimer, 1972; Wagner et al., 1977; Fitzgerald and Gleadow, 1988) still provides a powerful approach to determine exhumation rates from geochronological data collected along steep elevation profiles. However, it has to be kept in mind that this method is prone to potentially large errors for the cases where the critical closure isotherms were not planar during the time of exhumation (Stüwe et al., 1998; Stüwe and Hintermüller, 2000). However, if this requirement is not met, the calculation from age-elevation trends may easily result in false conclusions about cooling and exhumation rates in the upper crust, as it was recently shown for instance by a study from the Eastern Alps (Wölfler et al., 2012).

In this study we aim to unravel the yet constrained thermal history of the Polinik and Kreuzeck Blocks (Staufenberg, 1987; Wölfler et al., 2008) – two Austroalpine units to the southeast of the Tauern Window that are bound by steep fault zones. For this purpose we provide an original dataset comprising new Ar/Ar ages on micas and new ZFT- and AFT ages from bedrock samples. The new data are used to better quantitatively constrain the cooling of the samples from the investigated tectonic units at <450°C, corresponding to the middle to upper crustal levels. In addition to the 'conventional' inverse modelling procedure by using HeFTy software (Ketcham, 2005), we employ also a transdimensional inverse thermal history modelling approach for multiple samples recently introduced by Gallagher (2012). Perhaps the main advantage of the new modelling approach is its ability to consider simultaneously all data from an age-elevation profile, and moreover, it allows calculation of paleo-geothermal gradients for the time sections between the oldest and the youngest ages in the age-elevation profile. Our new data from three thermochronometers, integrated with published data and new modelling strategies, enables us to reconstruct ~300 Ma of thermal history in the ~450 to 60°C temperature range, and provide new insights into final cooling stages of Austroalpine units that have implications for the evolution of the Eastern Alps.

2. Geological Setting

To a large extent the European Alps and in particular the Eastern Alps are composed of units derived from the Adriatic microplate, the Penninic oceanic realm and the European continent (Figs. 1, 2). The Austroalpine and Southalpine units represent the Adriadic microplate and the units derived from the Penninic oceanic realm are mainly exposed in tectonic windows (Fig. 2).

The Penninic units were overthrusted by the Austrolpine units in Cretaceous and Eocene times (e.g. Neubauer et al., 1999; Schmid et al., 2013). During the lateral tectonic extrusion of the Eastern Alps in Oligocene-Miocene times (e.g. Ratschbacher et al., 1991a, b; Wölfler et al., 2011) the footwall Penninic units exposed in the Tauern Window (Figs. 2, 3), were tectonically exhumed from below the Austroalpine hanging wall (Frisch et al., 1998, 2000). The Austroalpine units can be subdivided into Lower and Upper Austroalpine nappes (e.g. Schuster et al., 2013), which experienced a complex geological history from the Paleozoic to the Cenozoic era. The Lower Austroalpine units overlie the Penninic units and are mainly exposed at the border of the Tauern Window (Fig. 3). The Upper Austroalpine units are composed of several nappe sys-

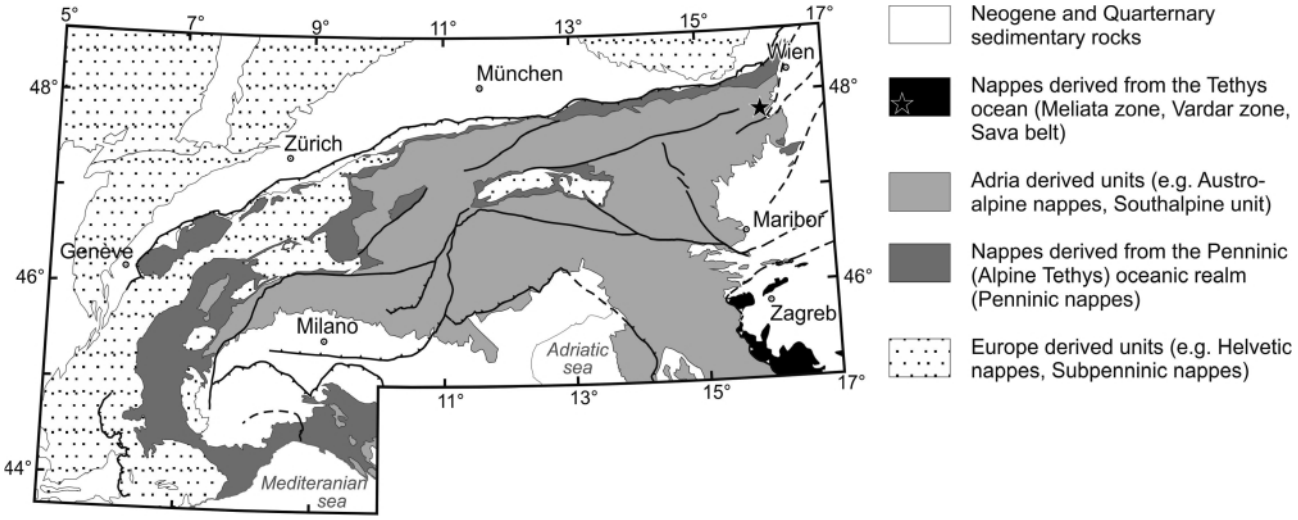

Figure 1: Tectonic map and paleogeographic units of the European Alps according to Schmid et al. (2004) (modified after Schuster et al., 2013).

tems (e.g. Schuster et al., 2013).

The area of investigation, situated within the Kreuzeck Mountains, covers a part of the Austroalpine units located to the southeast of the Tauern Window (Figs. 2, 3). It consists of polymetamorphic rocks which were overprinted from the Devonian to the Cretaceous (e.g. Hoinkes et al., 1999; Neubauer et al., 1999). A subvertical fault zone, referred to as the Ragga-Teuchl fault, separates the study area into two units that differ in their structural and metamorphic history (Fig. 3). The Ragga-Teuchl fault formed during the Oligocene and displays both ductile and brittle deformation and separates the Polinik Complex in the North from the Strieden Complex in the south (Hoke, 1990). Later on, during the lateral extrusion in the Miocene (Ratschbacher et al., 1991b) additional steeply dipping faults developed along the boundary of the recent Kreuzeck Mountains, thus forming a northern and southern block here referred as Polinik and Kreuzeck Blocks, respectively (Fig. 3).

The Polinik Block is part of the Koralpe-Wölz nappe system (Fig. 3), an Upper Austroalpine nappe system, which experienced a metamorphic imprint under high-amphibolite to eclogite facies conditions during the Eo-Alpine metamorphism (Schuster et al. 2001, 2004; Schmid et al., 2004). Published geochronological data from the Polinik Block include Cretaceous K/Ar- and Ar/Ar ages (~127 to ~67 Ma) on white mica and biotite (Oxburgh et al., 1966; Lambert, 1970; Hoke, 1990; Dekant, 2009), ZFT ages of ~45 to ~30 Ma, AFT ages of ~23 to ~7 Ma and apatite (U-Th)/He ages of ~17 to ~11 Ma (Dunkl et al., 2003; Staufenberg, 1987; Wölfler et al., 2008) (Fig. 4).

The Kreuzeck Block is part of the Drauzug-Gurktal nappe system (Fig. 3) which experienced a metamorphic imprint only under anchizonal to lowermost greenschist facies conditions during the Eo-Alpine metamorphism, and still preserves Variscan and Permian assemblages and structures (Hoke, 1990; Schuster et al., 2001, 2004). K/Ar and Ar/Ar ages on white mica and biotite range from 337 to 141 Ma (Brewer & Jenkins, 1969; Brewer, 1970; Hoke, 1990; Dekant, 2009) (Fig. 4). ZFT and AFT ages range from 160 to 60 Ma (Dunkl et al., 2003; Wölfler et al., 2008), and from 30 to 19 Ma, respectively (Staufenberg, 1987; Wölfler et al., 2008) (Fig. 4). During the Oligocene the Kreuzeck Block was intruded by tonalitic, alkaline basaltic and shoshonitic dykes (Exner, 1976; Deutsch, 1984; Müller et al., 1992).

The difference in ZFT and AFT ages to the north and south of the Ragga-Teuchl fault has been interpreted to reflect normal faulting related to the lateral extrusion of the Eastern Alps during early- and middle Miocene times (Wölfler et al., 2008).

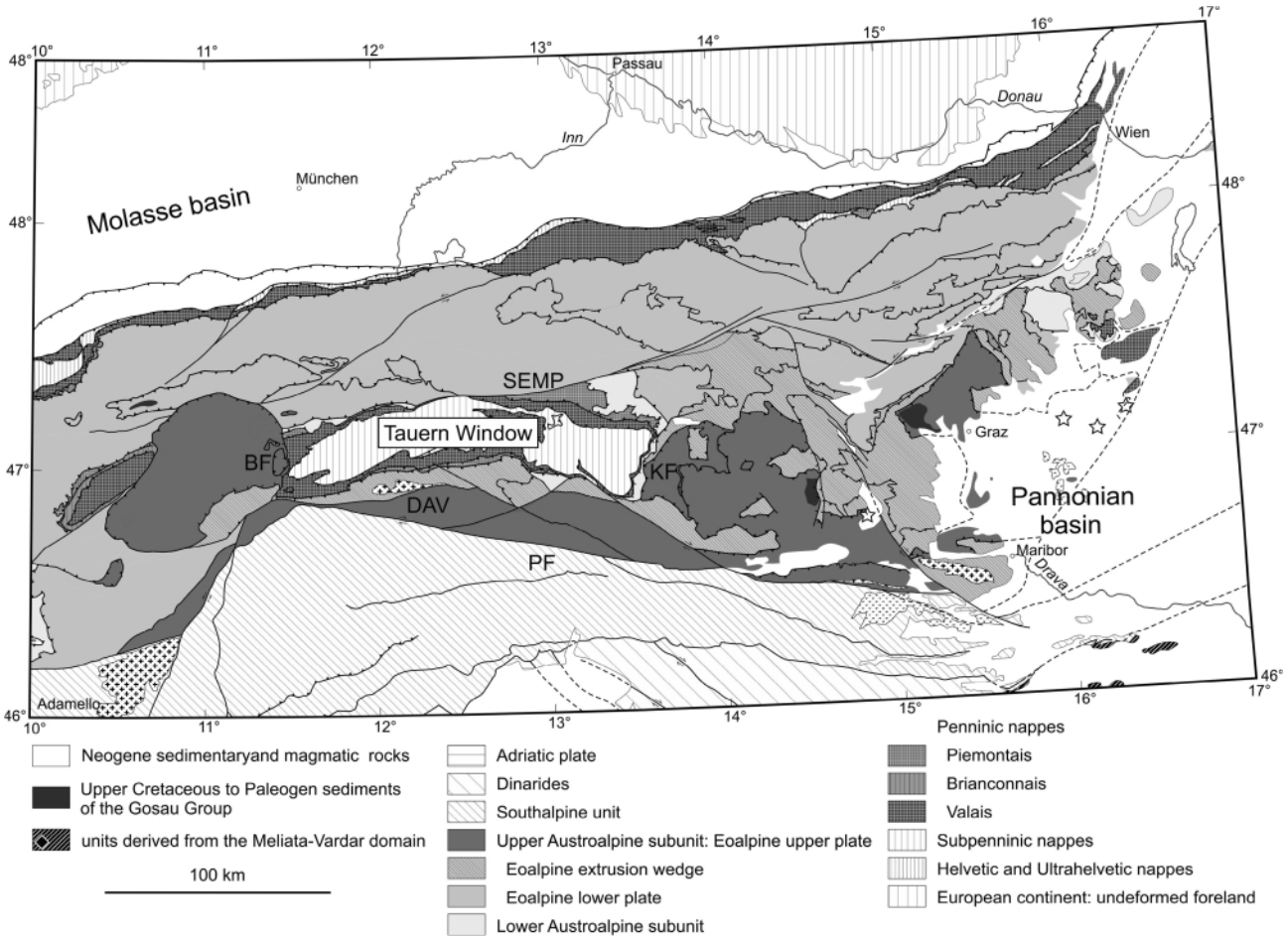

Figure 2: Tectonic map of the Eastern Alps following the nomenclature of Schmid et al. (2004) (modified after Froitzheim et al., 2008). BF: Brenner normal fault; KF: Katschberg normal fault; DAV: Defereggen-Antholz-Vals fault; SEMP: Salzach-Ennstal-Mariazell-Puchberg fault; PF: Periadriatic fault system; ZW: Zwischenbergen-Wöllatratten fault; RTF: Ragga-Teuchl fault; MV Mölltal fault.

Brittle deformation along the Ragga-Teuchl fault during the Oligocene to early Miocene is documented by Rb/Sr and K/Ar ages on cataclasites ranging from 32 to 30 and 23 to 22 Ma, respectively (Kralik et al., 1987).

Available geochronological data and the overall fault pattern suggest that the Ragga-Teuchl fault is structurally and temporally linked with the exhumation of the Tauern Window and associated faulting activity that affected the study area and the whole Eastern Alps during the Miocene lateral extrusion (e.g. Frisch et al., 2000; Scharf et al., 2013; Schmid et al., 2013; Wölfler et al., 2008, 2011, 2012). The fault zones that are in temporal and structural connection with the Ragga-Teuchl fault (Figs. 2, 3) are briefly described as follows: The Katschberg and Brenner fault zones border the Tauern Window in the east and west, respectively (Fig. 2), and are largely responsible for the exhumation of the Penninic footwall units during early to late Miocene times (e.g. Selverstone, 1988; Genser and Neubauer, 1989; Fügenschuh et al., 1997; Scharf et al., 2013; Schmid et al., 2013). The southern boundary of the Eastern Alps is represented by the Periadriatic fault system, separating the Austroalpine and Southalpine units (Fig. 2). Geochronological and structural data show that the Periadriatic fault system was dominated by strike slip deformation since the Oligocene (Müller et al., 2000; Mancktelow et al., 2001) and changed to transpressive deformation during the late Miocene until present (e.g. Polinski and Eisbacher, 1992; Fodor et al., 1998; Caparoli et al., 2013). The Mölltal fault forms a subvertical, structural lineament with a length of ~100 km (Fig. 3) that was interpreted to act as a stretching fault (Kurz and Neubauer, 1996; Scharf et al., 2013) and was mainly active in the early- to middle Miocene (Wölfler et al., 2008; Scharf et al., 2013). The Defereggen-Antholz-Vals fault system (DAV) represents an ~80 km long SSW-

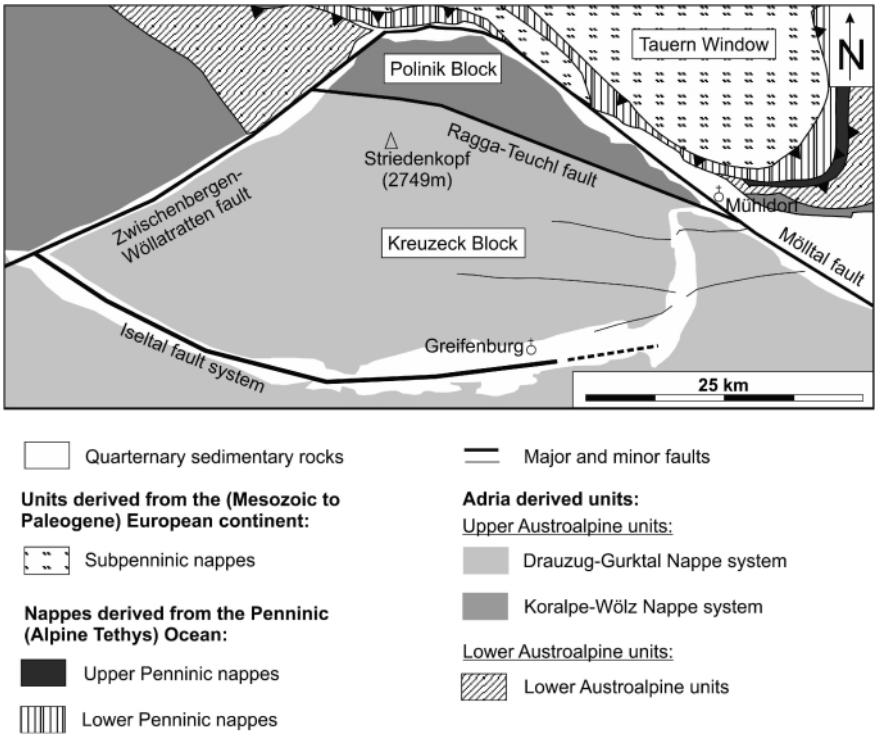

Figure 3: Simplified tectonic map of the study area and neighbouring units (modified after Linner et al., 2008 and Schuster et al., 2013).

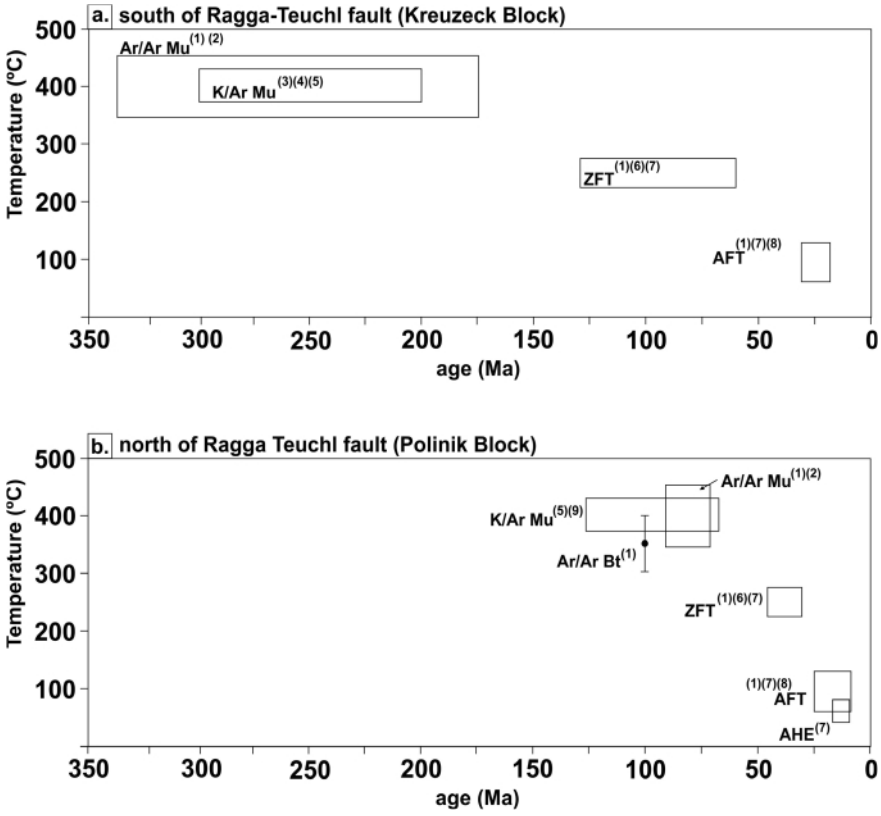

Figure 4: Geo- and thermochronological data in the study area. The data are from: (1) this study; (2) Dekant (2009); (3) Brewer and Jenkins (1969); (4) Brewer (1970); (5) Hoke (1990); (6) Dunkl et al. (2003); (7) Wölfler et al. (2008); (8) Staufenberg (1987); (9) Lambert (1970). For closure temperature ranges we adopted the following values: K/Ar muscovite: ~430-375°C (Hames and Bowring, 1994; Kirschner et al., 1996); Ar/Ar muscovite: ~450-350°C (Hames and Bowring, 1994; Kirschner et al., 1996; Lips et al., 1996; Harrison et al., 2009); Ar/Ar biotite: 400-300°C (Grove and Harrison, 1996; Villa, 1998); zircon fission track: 300-200°C (Wagner and van den haute, 1992); apatite fission track: 120-60°C (Green et al., 1986).

striking fault (Fig. 2) which changed its kinematics from sinistral to dextral deformation in the Oligocene at ~30 Ma (Mancktelow et al., 2001). The Zwischenbergen-Wöllatratten fault offsets the DAV and the Ragga-Teuchl fault by ~20 km (Scharf et al., 2013), so that the Ragga-Teuchl fault represents the eastern continuation of the DAV fault (Scharf et al., 2013) (Fig. 2).

3. Methods

3.1 Sample description and sampling strategy

The samples collected for this study are mainly ortho- and paragneisses, pegmatites and schists that mainly contain quartz, muscovite, biotite and garnet. For Ar/Ar analysis we collected six samples that are briefly described as follows. Three samples were collected from the Polinik Block. Sample K80 was obtained from a pegmatitic vein in an eclogitic host rock. Sample K64 is a graphitic garnet micaschist. The microtexture exhibits idiomorphic garnets with pressure shadows filled with quartz, muscovite, biotite and chlorite (Fig. 5a). Sample K352 is a coarse-grained micaschist rich in staurolite. The garnets are idiomorphic and the strain shadows are mainly filled with quartz that shows straight grain boundaries, partly forming equilibrium fabrics (Fig. 5b). The large staurolite crystals are mainly hypidiomorphic and crosscut the foliation (Fig. 5b). Two samples from the Kreuzeck Block (K396, K397) are from a large porphyric orthogneiss. The microtextures show large feldspar porphyroclasts that are surrounded by quartz, muscovite and sometimes biotite (Figs. 5c, d). Sample K398 from the Kreuzeck Block is an orthogneiss composed of plagioclase- and feldspar porphyroclasts that are embedded in a matrix of quartz, muscovite and biotite (Fig. 5d). The matrix is rich in apatite and sphene. In places the biotites are retrogressed to chlorite.

For ZFT analysis we collected three samples from the Kreuzeck Block. These are two micaschists (samples K116, K143) and a tonalite body (sample K235) from the westernmost part of the study area (Fig. 6a) that has already been described by Exner (1956). In order to determine a detailed final cooling history of the study area, we focused our sampling campaign for AFT analysis on steep elevation profiles (Fig. 6). We collected bedrock samples from three profiles (one in the Polinik Block and two in the Kreuzeck Block; Fig 6a, profiles A, B, C), from elevations between 770 and 2390 m.a.s.l., with a vertical distance of 200 to 300 m between the sampled sites.

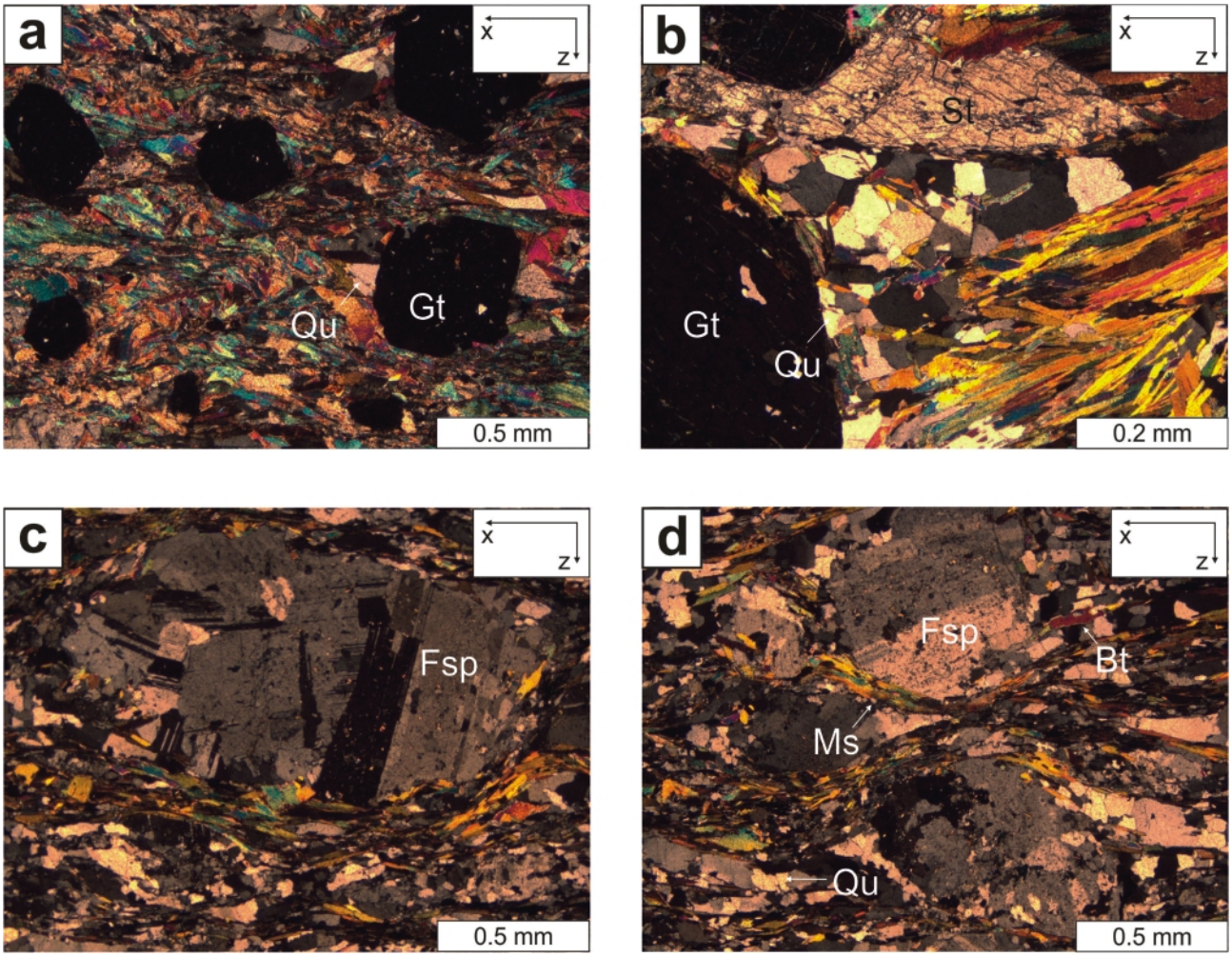

Figure 5: Thin section photographs illustrating microstructures of various rocks, from which micas were separated for Ar/Ar dating. For sample locations see Fig. 5 and Table 1. All photographs taken under crossed polarisers. Fsp: feldspar; Ms: muscovite; Qu: quartz; Gt: garnet; St: staurolite.

3.2 Analytical procedure

For Ar/Ar analysis pure mica concentrates were prepared from mica-rich fractions by using a Wilfley shaking table. After further enrichment on the Frantz magnetic separator, another step of purification was performed on a dry shaking table. The micas were then grinded in an agate mortar and ultrasonicated in acetone bath to remove inclusions and impurities. Final purification to >99 % was achieved by handpicking under a binocular. Pure mica concentrates were then loaded into glass tubes and irradiated together with sample monitors of known isotopic compositions in the nuclear reactor at the Nuclear Research Institute Řež in Prague. The irradiation J-values were

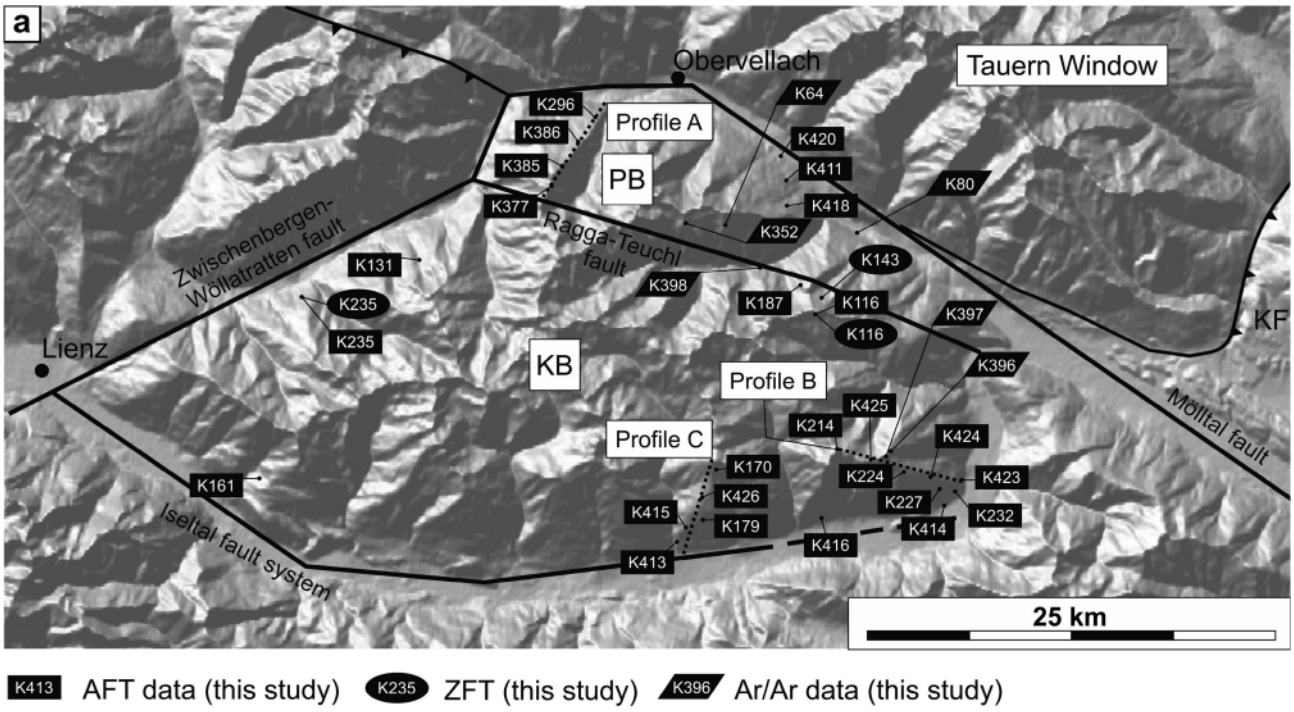

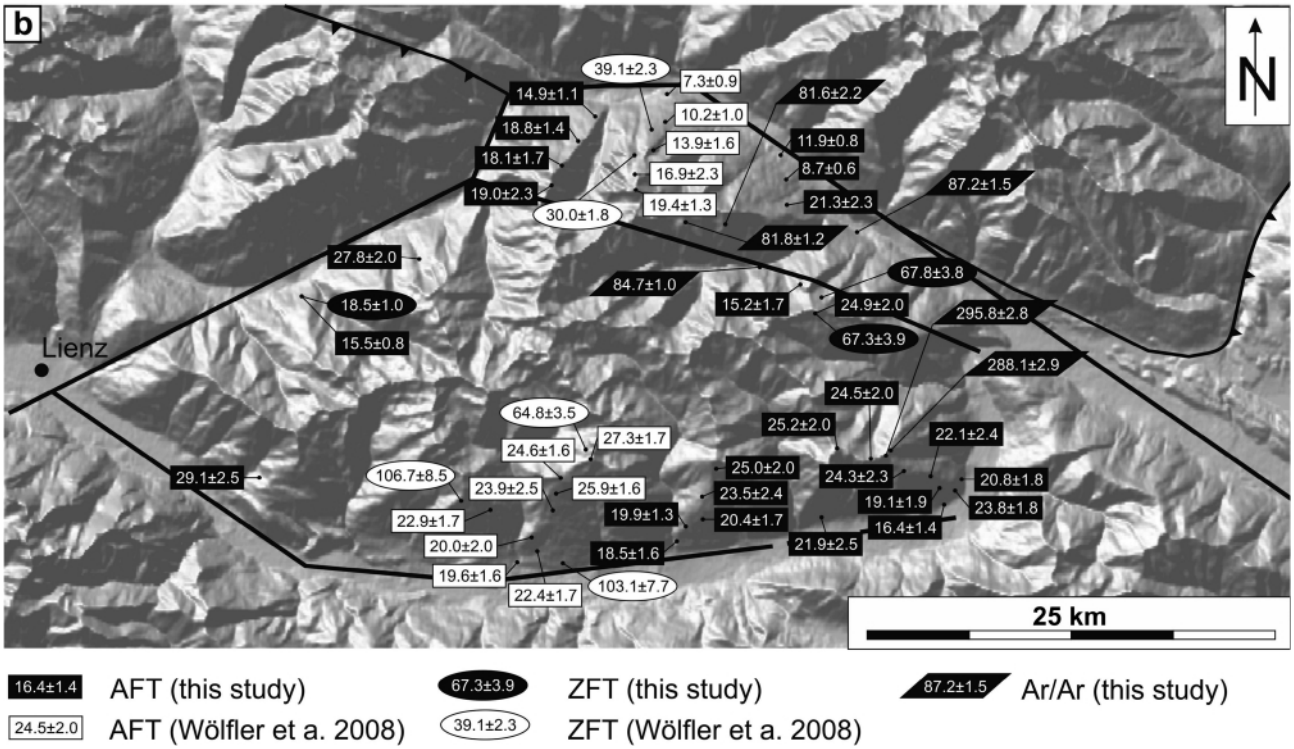

Figure 6: (a) Digital elevation model of the study area with sample locations and sample codes and the location of the age-elevation profiles A, B and C that have been used for thermal history models that are shown in Figures 7 and 8. KF: Katschberg normal fault; PB: Polinik Block; KB: Kreuzeck Block. (b) New- and published thermochronological data (Wölfler et al., 2008); for space reasons the AFT data of Staufenberg (1987) and ZFT data of Dunkl et al. (2003) are not shown in this figure but are incorporated in Fig. 4.

determined with international standards including muscovite Bern 4M (Burghele, 1987) and Fish Canyon sanidine (Renne et al., 1994; Jourdan and Renne, 2007). Ar/Ar-dating was conducted in the Central European Ar-Laboratory (CEAL) at the Geological Institute of the Slovak Academy of Science, Bratislava. Isotopic ages were calculated using decay constants reported by Steiger and Jäger (1977) and using the following correction factors for interfering isotopes: $^{40}Ar/^{36}Arair$ = 299± 1%; $^{36}Ca/^{37}Ca$ = 0.00027; $^{39}Ca/^{37}Ca$ = 0.00039; $^{40}K/^{39}K$ = 0.0254. Argon was released using the stepwise heating technique using a resistance furnace and analyzed on a VG-5400 Fisons noble-gas mass spectrometer following the analytical procedure of Frimmel and Frank (1998).

Apatite and zircon grains were separated using conventional magnetic and heavy liquid separation techniques. Unfortunately not all rocks contained enough zircon and/or apatites for fission track analysis. We used the external detector method (Gleadow, 1981) with low-uranium muscovite sheets (Goodfellow mica™) and the zeta calibration approach (Hurford and Green, 1983). Zircon mounts were etched in a KOH-NaOH eutectic melt at 215 °C (Gleadow et al., 1976) for 24 to 140 hours, whereby this time variation is dependent on the uranium content, age and the grade of metamictization of the individual grains. Apatite mounts were etched in 5.5 Mol HNO_3 for 20 sec at 21 °C (Donelick et al., 1999). Fission track ages were calculated with the program TRACKKEY version 4.1 (Dunkl, 2002). For the assessment of annealing kinetics in apatites we used Dpar values (mean diameters of etch figures on prismatic surfaces of apatite parallel to the crystallographic c-axis) (Burtner et al., 1994). Horizontal confined track lengths were corrected for c-axis orientation (Donelick et al., 1999).

Modelling of the low temperature thermal history based on AFT data was carried out using two different modelling programs - the conventionally used HeFTy (Ketcham, 2005) and the recently introduced QtQt software (Gallagher et al., 2005, 2009; Stephenson et al., 2006; Gallagher, 2012). For thermal history modelling with the HeFTy software (Ketcham, 2005) we used the annealing algorithm of Ketcham et al. (1999) and Dpar values as kinetic parameters. The QtQt sotware allows determining the thermal history of multiple samples and uses a Baysian transdimensional Markov chain inversion scheme (Gallagher et al., 2005, 2009; Gallagher, 2012). The main advantage of the QtQt modelling approach is that it incorporates all data from vertical age-elevation profiles. The thermal histories for all samples between the top and the bottom of the profiles are determined by using the elevation/depth differences. The offset parameters are the temperature difference between the highest and lowest elevation samples over time. The thermal history for samples between these two is obtained by linear interpolation, based on the difference in elevation. The temperature offset is not the paleo-geothermal gradient, however the temperature offset divided by the elevation difference between the uppermost and lowermost sample of the profile does provide information on the paleo-geothermal gradient. For more details about this modelling approach the reader is referred to the following publications: Stephenson et

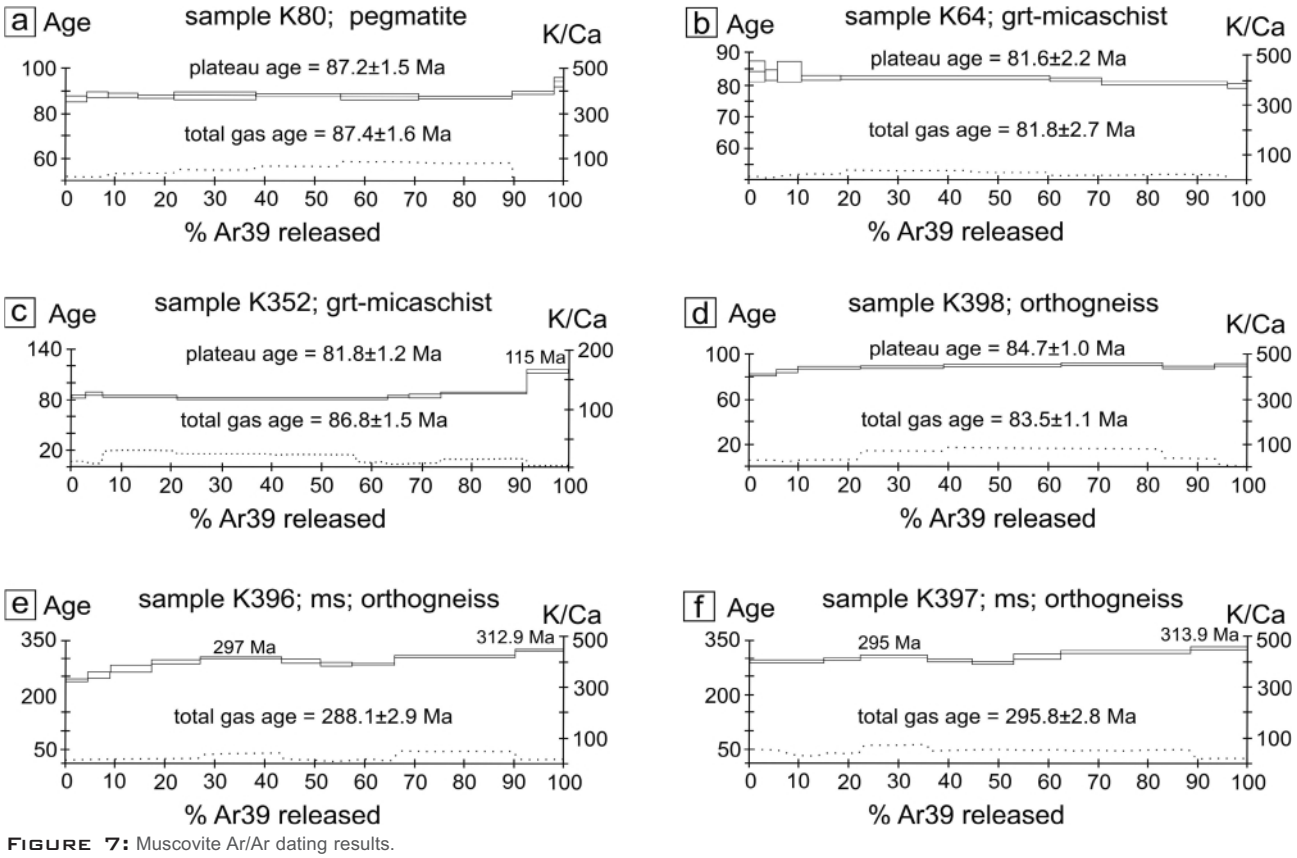

Figure 7: Muscovite Ar/Ar dating results.

sample code	elevation (m)	Longitude	Latitude	lithology	mineral	J	weight (mg)	Grain size (µm)	WM(P)A (Ma)	steps used	%39 Ar used	TGA (Ma)	%rad	IC-age* (Ma)	IC 40Ar/39Ar* intercept
K64	2250	46.883	13.198	garnet-mica-schist	mu	0.01510	7.9	80-160	81.6±2.2	6(10)	90	81.8±2.7	59-87	82±1	277±7
K80	670	46.879	13.279	pegmatite	mu	0.01510	5.2	500-2000	87.2±1.5	7(10)	85	87.4±1.6	92-98	88±1	324±30
K352	2190	46.884	13.182	garnet-mica-schist	mu	0.01525	8.1	80-200	81.8±1.2	4-7(10)	47	86.8±1.5	90-95	*	na
K396	2050	46.795	13.301	orthogneiss	mu	0.01525	7.7	80-200				288.1±2.9	95-98	337±18	*
K397	1910	46.790	13.05	orthogneiss	mu	0.01525	7.4	80-200				295.8±2.8	20-26	313±19	*
K398	990	46.866	13.235	orthogneiss	mu	0.01525	7.0	80-200	84.7±1.0	5(10)	61	83.5±1.1	92-95	89±3	*

Table 1: Summary of Ar/Ar data. J: irradiation parameter; WM(P)A: weighted mean plateau age; TGA: total gas age; %rad: range of radiogenic content of all steps; IC: isotope correlation; * only plateau steps were used for IC, meaningless results omitted; na: not analyzed. Latitude and longitude coordinates are given in the WGS 84 datum.

al., (2006); Hopcroft et al., (2007); Charvin et al., 2009; Gallagher et al., 2005, 2009; Gallagher, 2012).

4. Results

In total, we report six Ar/Ar, three ZFT and twenty-six AFT ages. The sample locations and results are shown in Fig. 6 and in Tables 1, 2 and 3.

4.1 Ar/Ar dating results

From four samples plateau ages have been determined (Figs 7a-d). In general, the samples from the Polinik Block revealed Cretaceous ages between ~87 and ~82 Ma. In contrast, two samples from the Kreuzeck Block display Permian ages of ~295 and ~288 Ma and one sample revealed a Cretaceous age of ~85 Ma (Fig. 7d).

Sample K80 from the Polinik Block yielded a well-defined plateau age of 87.2±1.2 Ma (Fig. 7a, Table 1). The last two temperature steps give slightly elevated ages of 94 and 89 Ma. These may be the relics of incompletely reset diffusion domains.

Sample K64 is a graphitic garnet micaschist from the Polinik Block with a plateau age of 81.6±2.2 Ma (Fig. 7b). The age step pattern shows signs of weak impregnation of excess argon, but this may be an effect of the larger errors at the lowermost temperature steps.

The Polinik Block sample K352 yielded a plateau age of 81.8±1.2 Ma. However, an age of 115 Ma is obtained for the highest temperature step (Fig. 7c) that indicates domains with excess argon or relics of older generation of muscovites.

The orthogneiss sample K398 from the Kreuzeck Block comes from the south of the Ragga-Teuchl fault and shows a well-defined plateau age of 84.7±1.0 Ma (Fig. 7d). Probably due to diffusive loss of argon in the outermost domains of the grains, the lowest temperature steps show slightly younger ages.

Samples K396 and K397 from the Kreuzeck Block are discussed together as they were taken from the same large porphyric orthogneiss body and show similarities in their texture and Ar-release patterns. Both samples exhibit a saddle shape rather than a plateau type pattern. The samples gave total gas ages of 288.1±2.9 and 295.8±2.8 Ma for K396 and K397, respectively (Figs. 7e, f). At the highest temperature step apparent ages of both samples are equal within error (312.9±1.1 Ma for sample K396 and 313.8±1.0 Ma for sample K397) (Figs. 7e, f).

4.1 Zircon- and apatite fission track results

All ZFT and AFT samples pass the chi-square test at a 95 % confidence interval and

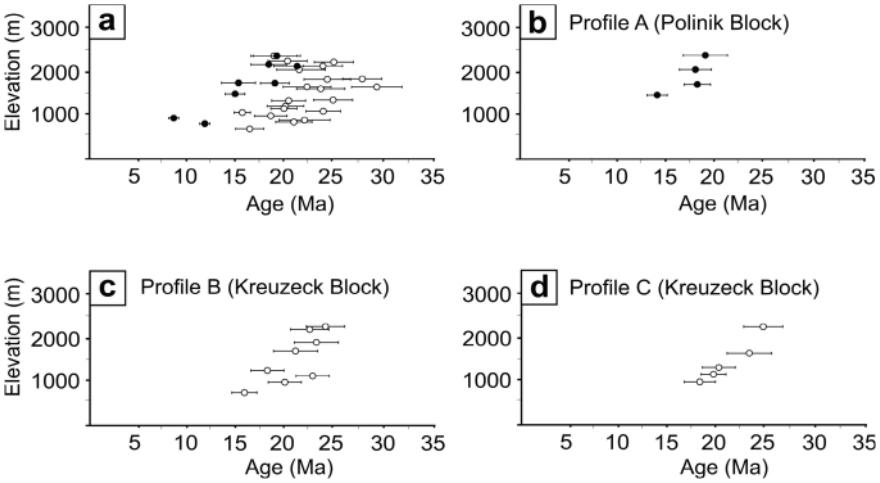

Figure 8: (a) Age-elevation relationships of all AFT samples in the study area. Black circles: samples from the Polinik Block; white circles: samples from the Kreuzeck Block. (b) Age-elevation relationship of samples from profile A in the Polinik Block. (c) and (d) Age-elevation relationship of samples from profile B and C from the Kreuzeck Block. The samples from these profiles have been used for transdimensional thermal modelling that is shown in Fig. 8.

sample code	long.	lat.	elevation (m a.s.l.)	n	ρ_s	N_s	ρ_i	N_i	ρ_D	Nd	P(χ2) (%)	Age (Ma)	±1σ (Ma)
K116	46.848	13.257	1300	20	101.723	955	64033	610	6873	3089	99.2	67.9	4.0
K143	46.862	13.292	1040	20	50.828	1016	31468	629	6825	3089	96.0	67.8	3.8
K235	46.871	13.007	1050	20	52.816	604	121	1382	6794	3089	66.7	18.5	1.0

Table 2: Summary of zircon fission track data. n: number of dated apatite crystals; ρ_s/ρ_i: spontaneous/induced track densities (x10^5 tracks/cm^2); Ns/Ni: number of counted spontaneous/induced tracks; ρd: dosimeter track density (x10^5 tracks/cm^2); Nd: number of tracks counted on dosimeter; P(χ^2): probability obtaining chi-square (χ^2) value for n degrees of freedom (where n is number of crystals minus 1); age ± 1σ is central age ± 1 standard error (Galbraith and Laslett, 1993); ages were calculated using zeta calibration method (Hurford and Green, 1983); glass dosimeter CN-2. Latitude and longitude coordinates are given in the WGS 84 datum.

are reported as central ages with 1 sigma errors (Tables 2, 3). Two micaschist samples from the Kreuzeck Block yielded ZFT ages of 67.3±3.9 and 67.8±3.8 Ma (samples K116 and K143). The youngest ZFT age of 18.5±1.0 Ma was determined from the tonalite body from the westernmost part of the study area (Fig. 6b).

In general, the Kreuzeck Block shows older AFT ages (29.1± 2.5 to 16.41.4 Ma) than the Polinik Block (21.3±2.3 to 8.7±0.6 Ma) and the samples follow an age-elevation trend (Table 3, Figs. 6b, 8). Track length distributions were measured in ten samples (Table 3). The mean confined track lengths (MTL) vary between 13.84±1.3 µm (sample K296) and 13.14±1.14 µm (sample K426). All samples are characterized by long MTL (>13 µm) and a unimodal distribution suggesting fast cooling through the partial annealing zone. Dpar values range from 1.9 to 1.8 µm (Table 3), pointing to a homogeneous chemical composition of the samples, typical for a fluorine-apatite composition.

4.3 Thermal history modelling

For the tonalite sample K235 from the Kreuzeck Block we performed the inverse thermal history modelling with the HeFTy

sample code	elevation (m)	Longitude	Latitude	N	ρ_s	N_s	ρ_i	N_i	ρ_D	Nd	P(χ2) (%)	Age (Ma)	±1σ (Ma)	MTL (µm)	SD (µm)	N(L)	Dpar (µm)
K116	1300	46.848	13.257	25	0.977	191	3587	444	5685	11328	95.0	24.9	2.0				1.92
K131	1830	46.869	13.032	24	1.299	177	5052	727	7091	12503	74.2	27.8	2.0	13.74	1.14	100	1.83
K161	1631	46.781	12.945	25	0.933	127	4174	566	8055	15118	100.0	29.1	2.5				1.87
K170	2275	46.812	13.199	25	0.889	208	4347	1012	7549	15118	93.4	25.0	2.0	13.44	1.27	80	1.92
K179	1285	46.766	13.190	25	0.889	93	5457	528	7171	12503	96.9	20.4	1.7				1.83
K187	1728	46.859	13.257	25	0.655	148	4121	659	7208	15118	99.8	15.2	1.7				1.87
K214	2270	46.792	13.271	25	0.760	212	3380	922	6896	12503	99.7	25.2	2.0				1.86
K224	1860	46.785	13.306	25	0.714	137	3487	678	7492	14233	96.7	24.3	2.3	13.30	1.14	97.0	1.85
K227	1200	46.778	13.323	30	1.118	162	7047	1015	7412	14233	100.0	19.1	1.9				1.88
K232	1075	46.776	13.329	25	1.120	195	5256	811	6935	12503	57.5	23.8	1.8				1.79
K235	1050	46.871	13.007	25	0.788	93	5225	808	8376	11328	99.0	15.5	0.8	13.76	1.35	67	1.84
K296	1485	46.918	13.132	25	0.949	114	7592	737	5900	14233	87.8	14.9	1.1	13.84	1.27	76	1.90
K377	2390	46.896	13.108	25	1.013	123	6250	664	7233	15118	98.4	19.0	2.3	13.62	1.28	83	1.85
K385	2102	46.907	13.119	25	1.145	117	7601	772	7407	14233	91.3	18.1	1.7				1.81
K386	1726	46.914	13.126	25	1.436	111	7058	771	8118	15118	85.2	18.8	1.4				1.82
K411	930	49.911	13.218	25	0.760	89	8795	1020	6211	11328	99.1	8.7	0.6				1.88
K413	985	46.759	13.185	24	0.709	120	2723	634	6299	11328	94.5	18.5	1.6	13.78	1.26	73	1.81
K414	640	46.767	13.295	25	0.732	124	4452	752	6167	11328	100.0	16.4	1.4	13.82	1.20	93	1.75
K415	1130	46.761	13.188	25	1.515	122	5058	639	6474	11328	89.8	19.9	1.3				1.83
K416	870	46.765	13.261	25	0.912	136	3556	530	5291	11328	100.0	21.9	2.5				1.85
K418	2165	46.892	13.231	25	1.378	152	5752	661	5511	11328	95.9	21.3	2.3	13.79	1.21	78	1.88
K420	770	46.921	13.208	26	1.121	88	8321	1015	5467	11328	91.5	11.9	0.8				1.84
K423	870	46.784	13.344	25	1.281	171	5481	781	5906	11328	100.0	20.8	1.8				1.76
K424	1640	46.784	13.314	25	1.274	240	5481	1024	5905	11328	100.0	22.1	2.4				1.83
K425	2130	46.788	13.287	27	1.378	307	5409	1092	5973	11328	100.0	24.5	2.0				1.86
K426	1630	46.774	13.196	25	0.893	240	3948	1089	6610	12503	91.0	23.5	2.4	13.14	1.14	100	1.80

Table 3: Summary of apatite fission track data. n: number of dated apatite crystals; ρ_s/ρ_i: spontaneous/induced track density (x10^5 tracks/cm^2); Ns/Ni: number of counted spontaneous/induced tracks; ρd: dosimeter track density (x10^5 tracks/cm^2); Nd: number of tracks counted on dosimeter; P(χ^2): probability obtaining chi-square value (χ^2) for n degree of freedom (where n is number of crystals minus 1); MTL: mean track length; SD: standard deviation of track length distribution; N(L): number of horizontal confined tracks measured; Dpar: average etch pit diameter of fission tracks; age ± 1σ is central age ± 1 standard error (Galbraith and Laslett, 1993); ages were calculated using zeta calibration method (Hurford and Green, 1983); glass dosimeter CN-5. Latitude and longitude coordinates are given in the WGS 84 datum.

	sample	elevation (m)	difference (m)	age (Ma)	temp. Offset (°C)	thermal gradient (°C/km)
Profile A (Polinik Block)	K377	2390		19.0		
	K297	1485	905	14.9	42	46
Profile B (Kreuzeck Block)	K214	2270		25.2		
	K414	640	1630	16.4	76	47
Profile C (Kreuzeck Block)	K170	2275		25.0		
	K413	985	1290	18.5	56	43

Table 4: Parameters used for the calculation of the paleo-geothermal gradients.

software (Ketcham, 2005). Based on zircon U-Pb data, Dekant (2009) calculated a crystallization age of 31 Ma for this sample. As a starting point we assumed a temperature range of 750-950 °C for magma emplacement as inferred from zircon saturation in a silica melt and numerical modelling (Bellieni et al., 1984; Steenken et al., 2002). The HeFTy model suggests fast exhumation at a rate of 60°C/Ma since the intrusion of the tonalite at ~31 Ma to ~13 Ma, followed by thermal stagnation (Fig. 9a).

Transdimensional thermal history modelling with the QtQt software was performed on three steep elevation profiles that comprises the AFT ages with 1 sigma errors, the mean track length distributions and Dpar values. Profile A is from the Polinik Block and includes samples K296, K385, K386 and K387 (Fig. 6a). Profiles B (samples K214, K224, K 227, K232, K414, K423, K424, K425) and C (samples K170, K179, K413, K415, K426) are from the Kreuzeck Block (Fig. 6a). Rapid cooling through the apatite partial annealing zone (120 to 60°C, Green et al., 1986) for the northern profile in the Polinik Block occurred between ~17 and ~14 Ma (Fig. 9b). In contrast, the samples from the Kreuzeck Block cooled through the apatite partial annealing zone already during Oligocene and early Miocene times approximately between ~30 and ~22 Ma (Figs. 9c, d). The summary plots of the track length data for selected samples display the observed data and the predictions from the thermal history models (Figs. 9e-g) that are in good agreement. The temperature offset between the upper- and lowermost samples of the profiles are shown in Figs. 9 h–j. It should be noted that the temperature offset is not the paleo-geothermal gradient. However, with the knowledge of the vertical distance between the upper and the lower sample the paleo-geothermal gradient can be straightforwardly calculated. We emphasize that the calculated paleo-geothermal gradient covers only the time period of the oldest and youngest age of the profile. The paleo-geothermal gradient for the Polinik profile (Profile A) is 46 °C/km for the time between ~19 and ~15 Ma, and 47 and 43°C/km for the profiles B and C, respectively, in the two Kreuzeck Block profiles for the time between ~25 and ~16 Ma. The details for the calculations are shown in Table 4.

5. Interpretation and discussion

Muscovite Ar/Ar plateau ages from the Polinik Block and for one sample of the Kreuzeck Block range between ~87 and ~82 Ma (Fig. 7a-d). The microtextures show mainly well-preserved high-pressure assemblages like unaltered garnets, no or little chloritisation and idiomorphic staurolite (Fig. 5). Therefore we interpret the detected time interval as the time of post-metamorphic cooling that followed thermal maximum of the high pressure Eo-Alpine metamorphism with a peak at ~90 Ma (e.g. Thöni et al., 2006). We interpret the Cretaceous cooling as a result of overall extension that has been observed in the Austroalpine nappe stack (e.g. Froitzheim et al., 1997, 2012; Fügenschuh et al., 2000; Liu et al., 2001; Kurz and Fritz, 2003). The exhumation of the Eo-Alpine high pressure wedge is due to thrusting in the lower part and normal faulting in the upper part of the Austroalpine nappe pile (Sölva et al., 2005; Schuster et al., 2004, 2013) but still in a compressional environment. This process was associated with the formation of the Gosau sedimentary basins between Late Cretaceous and early Eocene (Wagreich, 1995; Froitzheim et al., 1994; Neubauer et al., 1995, 2000) that were deposited in a transpressional regime (Ortner, 2007).

Two samples from the Kreuzeck Block display Permian total gas Ar/Ar ages (Fig. 7e, f). At the highest temperature steps the data display late Carboniferous ages that might represent the oldest domains which have retained Variscan argon age signature. The data are therefore considered as geologically meaningful, as they are consistent with late Carboniferous cooling ages reported for the Eastern Alps in general (e.g. Handler et al., 1997; Neubauer and Handler, 2000) and in particular for the study area (Hoke, 1990 and references therein). We suggest that the rather complex argon release spectra from the Kreuzeck Block are possibly related to both, late Variscan collapse in the late Carboniferous and to post-Variscan extension and cooling during the Permian (Schuster and Stüwe, 2008). The cooling in the Polinik Block occurred subsequent to peak metamorphic conditions during Eo-Alpine metamorphism. This extensional phase is associated with the orogenic collapse in the Late Cretaceous.

The Cretaceous ZFT ages (~68 and ~67 Ma) from the Kreuzeck Block are interpreted as recording cooling after the Eo-Alpine metamorphic peak. Our new data are consistent with other ages reported from large parts of the Austroalpine units that cooled through the ZFT partial annealing zone (300 to 200°C, Wagner and Van den Haute, 1992) before Cenozoic times (e.g. Dunkl et al., 2003; Fügenschuh et al., 1997; Hejl, 1997, 1998; Kurz et al., 2011; Luth and Willingshofer, 2008; Wölfler et al., 2008, 2010, 2012). The Miocene ZFT age of 18.5±1.0 Ma from the tonalitic intrusion in the western part of the study area (Fig. 6) is thus far the youngest ZFT age ever reported from this part of the Eastern Alps. Both, the Miocene ZFT- and AFT (15.5±0.8 Ma) ages from the tonalite as well as

the modelled cooling history (Fig. 9a) is in agreement with cooling histories of intrusive rocks along the Periadriatic fault, and collectively suggests that fast and continuous cooling at a rate of ~60°C/Ma occurred immediately after the Oligocene emplacement and lasted until the middle Miocene (Fig. 9a) (e.g. Fügenschuh et al., 1997; Stöckhert et al., 1999; Viola et al., 2001; Steenken et al., 2002; Most, 2003; Pomella et al., 2010).

The youngest AFT ages of 21.3±2.3 to 8.7±0.6 Ma are found in the Polinik Block (Fig. 6b, Table 3). These ages are similar to those from the eastern Tauern Window (e.g. Wölfler et al., 2008, 2012) and document contemporaneous cooling of the Penninic- and Austroalpine units during the middle Miocene. The oldest AFT ages are from the Kreuzeck Block and range between 29.1±2.5 and 18.5±1.6 Ma (Fig. 6b). This indicates

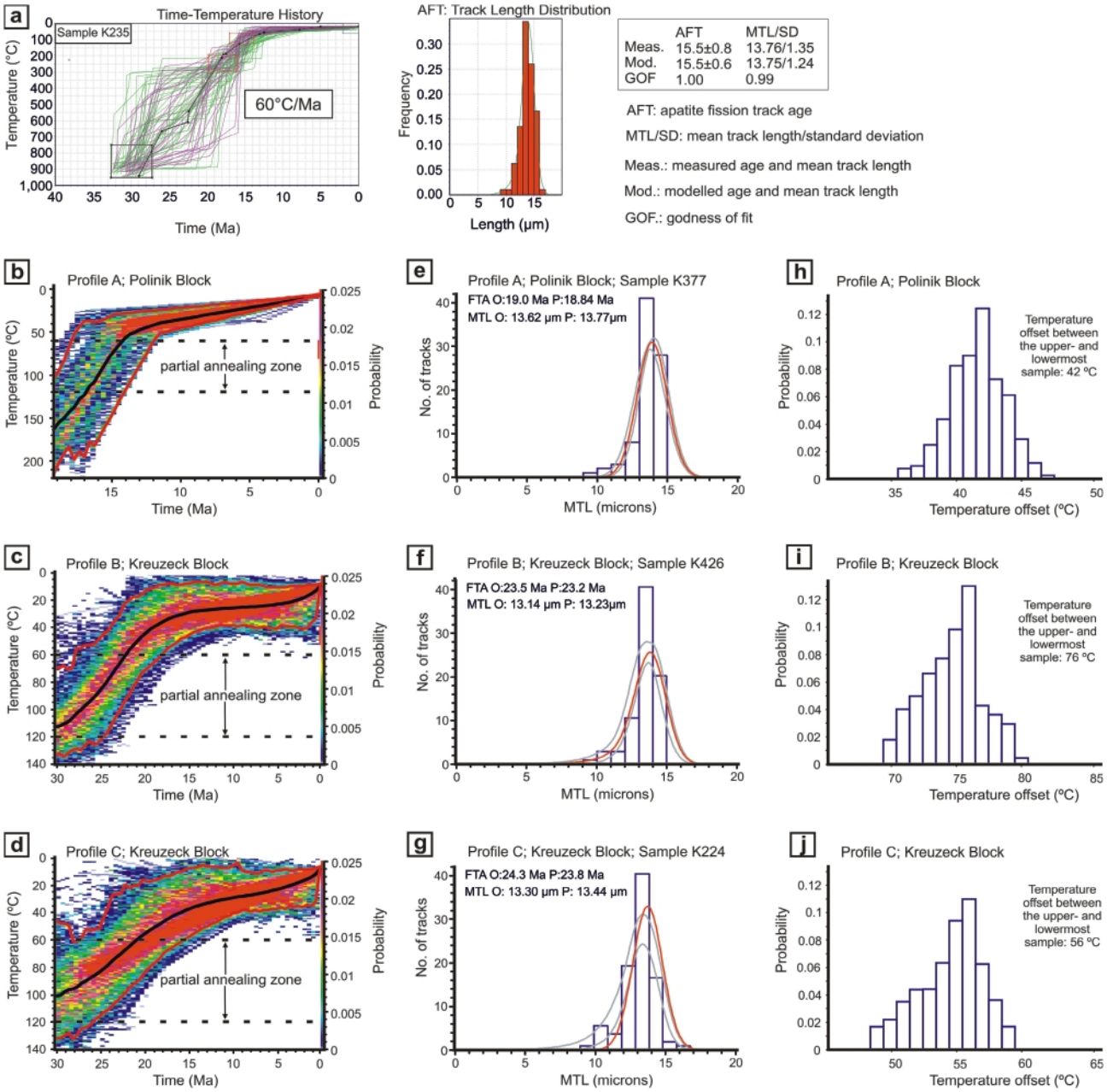

Figure 9: (a) Thermal history inverse model for the tonalite sample K235 using the software HeFTy (Ketcham, 2005). Input parameters: central AFT age with 1σ error; track length distributions, Dpar values as kinetic parameters. For starting conditions (black box) we choose a temperature range between 750 and 950 °C as magma emplacement temperature (Watson and Harrison, 1983; Bellieni et al., 1984; Steenken et al., 2002). The red boxes are the temperature range for ZFT ages (ZFT: 18.5±1.0 Ma) and the temperature range for AFT ages (AFT: 15.5±0.8 Ma). The blue box defines the final cooling to present-day temperatures of ~10 °C. Green paths: acceptable fits; red paths: good fits; black line: best fit solution. (a-d) The expected (weighted mean) thermal history (black line) and its probability distribution for transdimensional modelling of all samples from the Profiles A to C. The red lines are the 95 % credible intervals for the thermal history. The credible interval is the Bayesian form of the confidence interval (e.g. Bernardo and Smith, 2000; Gallagher, 2012). The scale on the right indicates the probability. (e-g) Model predictions for the thermal history of distinct samples from the profiles. The grey lines are the 95 % credible intervals for the predicted values. FTA is the fission track age, MTL is the mean track length in micrometers (O: observed, P: predicted). (h-j) The paleo-offset temperature as a function of probability (between the upper- and lowermost sample in a profile). Note: the paleo-offset temperature is not the paleo-geothermal gradient.

that cooling through the apatite partial annealing zone took place earlier in the Kreuzeck Block than in the northern Polinik Block (Staufenberg, 1987; Wölfler et al., 2008, 2012). The AFT ages show a positive trend in the age-elevation correlation in the whole study area (Fig. 8a), and in particular for the three selected profiles (Figs. 8b-d). To better constrain the cooling history we used these age elevation correlations for multiple thermal history modelling. The thermal history model of the Polinik Block suggests rapid cooling in the middle Miocene (Fig. 9a), which coincides with the timing of the lateral extrusion (Frisch et al., 2000). In contrast, the Kreuzeck Block had already cooled to near surface temperatures in the Oligocene and early Miocene (Figs. 9c, d). The same cooling pattern applies to the western part of the DAV, where ZFT ages record pre-Miocene cooling to the south and Miocene cooling to the north (Stöckhert et al., 1999; Steenken et al., 2002; Most, 2003; Luth and Willingshofer, 2008). If the Ragga-Teuchl fault is considered the eastern continuation of the DAV (Scharf et al., 2013; Schmid et al., 2013), it is likely that the crystalline blocks to the north and south of it exhibit similar thermal histories.

The onset of rapid cooling and exhumation in the Polinik Block occurred at ~20 Ma (Fig. 9b) (Wölfler et al., 2008). Roughly between 23 and 21 Ma the Southalpine intender started to indent in the Eastern Alps (Scharf et al., 2013; Schmid et al., 2013). Contemporaneously, the Southalpine lithosphere started to subduct beneath the Eastern Alps (Lippitsch et al., 2003; Horváth et al., 2006). The combination of these processes led to lateral extrusion in the Eastern Alps and doming of Penninic units in the Tauern Window (Ratschbacher et al., 1991b; Scharf et al., 2013). Therefore, the initiation of lateral extrusion at ~ 20 Ma is probably more related to the indentation of the southalpine intender, rather than subduction roll back beneath the Carpatians (Horváth et al., 2006). However, the influence of the retreating subduction zone increased at ~18 Ma and leads to the formation of intramontane basins to the east of the Tauern Window and enhanced fault activity (Wölfler et al., 2011).

To summarize, we suggest that the Ragga-Teuchl fault plays a key role during lateral extrusion. It marks the border between footwall and hanging wall units (Polinik- and Kreuzeck Blocks, respectively) that experienced different cooling histories between the Oligocene and middle Miocene.

By determining the offset temperature between the highest and lowest sample in the vertical profiles (Figs. 9h-j) we were able to calculate the paleo-geothermal gradient for the specific time frames. Our calculations reveal relatively high values (47 to 43 °C/km) from late Oligocene to middle Miocene times. We interpret the high values as a result of elevated heat flow in the vicinity of the Oligocene plutons (Sachsenhofer, 2001) and the rapid exhumation of hot Penninic rocks during the middle Miocene (e.g. Fügenschuh, 1995; Genser et al., 1996; Dunkl et al., 1998; Rantitsch, 2000; Sachsenhofer, 2001). Indeed, the occurrence of Oligocene dykes and veins (Deutsch, 1984; Müller et al., 1992) and the occurrence of plutonic rocks (Exner, 1956, 1976) may be responsible for an elevated heat flow in the study area.

6. Conclusions

By using new thermochronological data and thermal history modelling we were able to demonstrate different cooling histories of Austroalpine basement blocks southeast of the Tauern Window. The oldest Ar/Ar ages are found in the southern Kreuzeck Block where Eo-Alpine deformation and metamorphism did not completely reset the Variscan and Permian signature in the mica Ar/Ar system. In contrast, the northern Polinik Block displays Cretaceous Ar/Ar cooling ages that record rapid cooling subsequent to the thermal peak of Eo-Alpine metamorphism. Late Cretaceous ZFT ages from the Kreuzeck Block are also related to post-metamorphic cooling that goes along with an extensional phase that affected the whole Eastern Alps. AFT data and thermal history models suggest that cooling to near surface conditions occurred during Oligocene/early Miocene times for the Kreuzeck and during middle Miocene times for Polinik Block. Based on the temperature difference between the uppermost and lowermost samples of three age-elevation profiles we were able to calculate the paleo-geothermal gradient for Oligocene and middle Miocene times. The calculated relatively high values range from 47 to 43 °C/km and reflect the elevated heat flow during Oligocene magmatism and the exhumation of hot Penninic domains in the middle Miocene.

Acknowledgements

This study was supported by the German Science Foundation (DFG-project FR 610/22). The Manuscript received constructive and helpful reviews by Ralf Schuster and Bernhard Fügenschuh. We thank Christoph Glotzbach for discussions and a review of an earlier version of the manuscript.

References

Barbarand, J., Hurford, T. and Cartern, A., 2003. Variation in apatite fission track length measurement: implications for thermal history modeling. Chemical Geology, 198, 77–106. http://dx.doi.org/10.1016/S0009-2541(02)00423-0

Bellieni, G., Peccerillo, A., Poli, G. and Fioretti, A., 1984. The genesis of late Alpine plutonic bodies of Rensen and Monte Alto (Eastern Alps); inferences from major and trace element data. Neues Jahrbuch für Mineralogie – Abhandlungen, 149(2), 209–224.

Bernado, J.M. and Smith, A.F.M., 2000. Bayesian Theory. Wiley and Sons, 586 pp.

Brewer, M. and Jenkins, H., 1969. Excess radiogenic argon in metamorphic micas from the Eastern Alps, Austria. Earth and Planetary Science Letters, 6, 321–331. http://dx.doi.org/10.1016/0012-821X(69)90180-0

Brewer, M., 1970. K-Ar age studies in the Eastern Alps – the Oberostalpindecke of Kärnten. PhD Thesis, University of Oxford.

Burghele, A., 1987. Propagation of error and choice of standard in the 40Ar/39Ar technique. Chemical Geology, 66, 17–19.

Burtner, R.L., Nigrini, A. and Donelick, R.A., 1994. Thermochronology of Lower Cretaceous source rocks in the Idaho-Wyoming thrust belts. AAPG Bulletin, 78, 1613–1636.

Caporali, A., Neubauer, F., Ostini, L., Stangl, G. and Zuliani, D., 2013. Modeling surface GPS velocities in the Southern and Eastern Alps by finite dislocation at crustal depths. Tectonophysics, 2013, http://dx.doi.org/10.1016/j.tecto.2013.01.016.

Charvin, K., Gallagher, K., Hampson, G. and Labourdette, R., 2009. A Bayesian approach to infer environmental parameters from stratigraphic data 1: Methodology. Basin Research, 21, 5–25. http://dx.doi.org/10.1111/j.1365-2117.2008.00369.x

Carlson, W.D., 1990. Mechanisms and kinetics of apatite fission track annealing. American Mineralogist, 75, 1120–1139.

Dekant, C., 2009. Investigations on the magmatic and metamorphic history of the Kreuzeck Massif, Carinthia, Austria. Tübinger Geowissenschaftliche Arbeiten, Reihe A 75, 68 pp.

Deutsch, A., 1984. Young Alpine dykes south of the Tauern Window (Austria): A K-Ar and Sr isotope study. Contributions to Mineralogy and Petrology, 85, 45–57.

Dodson, M.H., 1973. Closure temperature in cooling geochronological and petrological systems. Contributions to Mineralogy and Petrology, 40, 259–274.

Donelick, R.A., Ketcham, R.A. and Carlson, W.D., 1999. Variability of apatite fission track annealing kinetics II: crystallographic orientation effects. American Mineralogist, 84, 1224–1234.

Dunkl, I., 2002. TRACKKEY: a windows program for calculation and graphical presentation of fission track data. Computers & Geosciences, 2, 3–12. http://dx.doi.org/10.1016/S0098-3004(01)00024-3

Dunkl, I., Grasemann, B. and Frisch, W., 1998. Thermal effect on upper plate during core-complex denudation: a case study from the Rechnitz Window, Eastern Alps. Tectonophysics, 297, 31–50. http://dx.doi.org/10.1016/S0040-1951(98)00162-0

Dunkl, I., Frisch, W. and Grundmann, G., 2003. Zircon Fission track thermochronology of the southeastern part of the Tauern Window and the adjacent Austroalpine margin, Eastern Alps. Eclogae Geologicae Helveticae, 96, 209–217.

Exner, C.H., 1956. Geologische Beobachtungen (1955) in der Kreuzeck-, Sadnig-, Rieserferner- und Reisseckgruppe (Kartenblätter 177, 180, 181, 182). Verhandlungen der Geologischen Bundesanstalt (Wien), 24–27.

Exner, C.H., 1976. Die geologische Position der Magmatite des periadriatischen Lineamentes. Verhandlungen der Geologischen Bundesanstalt, Wien, 3, 3–64.

Farley, K., 2000. Helium diffusion from apatite: general behavior as illustrated by Durango fluorapatite. Journal of Geophysical Research, 105, 2903–2914. http://dx.doi.org/10.1029/1999JB900348

Farley, K., 2002. (H-Th)/He dating: techniques, calibrations and applications. Mineralogical Society of America. Reviews in Mineralogy & Geochemistry, 47, 819–844. http://dx.doi.org/10.2138/rmg.2002.47.18

Fitzgerald, P.G. and Gleadow, A.J.W., 1988. Fission track geochronology, tectonics and structure of the Transantarctic Mountains in Northern Victoria Land, Antarctica. Isotope Geoscience, 73, 169–198. http://dx.doi.org/10.1016/0168-9622(88)90014-0

Fleischer, R.L., Price, P.B., Symes, E.M. and Miller, D.S., 1964. Fission track ages and track-annealing behavior of some micas. Science, 143, 349–151. http://dx.doi.org/10.1126/science.143.3604.349

Fleischer, R.L., Price, P.B. and Walker, R.M., 1965. Effects of temperature, pressure, and ionization on the formation and stability of fission tracks in minerals and glasses. Journal of Geophysical Research, 70, 1497–1502. http://dx.doi.org/10.1029/JZ070i006p01497

Fleischer, R.L., Price, P.B. and Walker, R.M., 1975. Nuclear Tracks in Solids. University of California Press, 605 pp.

Flowers, R.M., Shuster, D.L., Wernicke, B.P. and Farley, K.A., 2007. Radiation damage control on apatite (U-Th)/He dates from the Grand Canyon region, Colorado Plateau. Geology, 35(5), 447-450. http://dx.doi.org/10.1130/G23471A.1

Fodor, L., Jelen, B., Marton, E., Skaberne, D., Čar, J. and Vrabec, M., 1998. Miocene – Pliocene tectonic evolution of the Slovenian Periadriatic fault: Implications for the Alpine – Carpathian extrusion models. Tectonics, 17, 690–709. http://dx.doi.org/10.1029/98TC01605

Foeken, J.P.T., Persano, C., Stuart, F.M. and ter Voorde, M., 2007. Role of topography in isotherm perturbation: apatite (U-Th)/He and fission track results from the Malta tunnel, Tauern Window, Austria. Tectonics, 26. http://dx.doi.org/10.1029/2006TC002049

Frimmel, H.E. and Frank, W., 1998. Neoproterocoic tectonothermal evolution of the Garieb Belt and its basement, Namibia and South Africa. Precembrian Research, 90, 1–28. http://dx.doi.org/10.1016/S0301-9268(98)00029-1

Frisch, W., Kuhleman, J., Dunkl, I. and Brügl, A., 1998. Palinspastic reconstruction and topographic evolution of the Eastern Alps during late Tertiary tectonic extrusion. Tectonophysics, 297, 1–15. http://dx.doi.org/10.1016/S0040-1951(98)00160-7

Frisch, W., Dunkl, I. and Kuhlemann, J., 2000. Post-collisional orogen-parallel large-scale extension in the Eastern Alps. Tectonophysics, 327, 239–265. http://dx.doi.org/10.1016/S0040-1951(00)00204-3

Froitzheim, N., Schmid, S.M., and Conti, P., 1994. Repeated change from crustal shortening to orogen-parallel extension in the Austroalpine units of Graubünden. Eclogae Geologicae Helvetiae, 87, 559–612.

Froitzheim, N., Conti, P., and van Daalen, M., 1997. Late Cretaceous, synorogenic, low-angle normal faulting along the Schlining fault (Switzerland, Italy, Austria) and its significance for the tectonics of the Eastern Alps. Tectonophysics, 280, 267–293. http://dx.doi.org/10.1016/S0040-1951(97)00037-1

Froitzheim, N., Plašienka, D. and Schuster, R., 2008. Alpine tectonics of the Alps and Western Carpathians. In: T. McCann (ed.), the geology of Central Europe. Geological Society London Special Publication, Volume 2, 1142–1232.

Froitzheim, N., Weber, S., Nagel, T.J., Ibele, T. and Furrer, H., 2012. Late Cretaceous extension in the Northern Calcareous Alps (Schesaplana, rätikon, Switzerland and Austria). International Journal of Earth Sciences, 101, 1315–1329. http://dx.doi.org/10.1007/s00531-011-0717-4

Fügenschuh, B., 1995. Thermal and kinematic history of the Brenner area (Eastern Alps, Tyrol). PhD Thesis, ETH Zürich, Switzerland.

Fügenschuh, B., Seward, D. and Mancktelow, N., 1997. Exhumation in a convergent orogen: the western Tauern Window. Terra Nova, 9, 213–217.

Fügenschuh, B., Mancktelow, N.S. and Seward, D., 2000. Cretaceous to Neogene cooling and exhumation history of the Oetztal-Stubai basement complex, Eastern Alps; a structural and fission track study. Tectonics, 19, 905–918. http://dx.doi.org/10.1029/2000TC900014

Galbraith, R.F. and Laslett, G.M., 1993. Statistical models for mixed fission track ages. Nuclear Tracks and Radiation Measurements, 21, 459–470. http://dx.doi.org/10.1016/1359-0189(93)90185-C

Gallagher, K., 1995. Evolving temperature histories from apatite fission-track data. Earth and Planetary Science Letters, 136, 421-435.

Gallagher, K., Stephenson, J., Brown, R., Holmes, C. and Fitzgerald, P., 2005. Low temperature thermochronology and modelling strategies for multiple samples 1: vertical profiles. Earth and Planetary Science Letters, 237, 193–208. http://dx.doi.org/10.1016/0012-821X(95)00197-K

Gallagher, K., Charvin, K., Nielsen, S., Sambridge, M. and Stephenson, J., 2009. Markov chain Monte Carlo (MCMC) sampling methods to determine optimal models, model resolution and model choice for Earth Science problems. Marine and Petroleum Geology, 26, 535–535. http://dx.doi.org/10.1016/j.marpetgeo.2009.01.003

Gallagher, K., 2012. Transdimensional inverse thermal history modelling for quantitative thermochronology. Journal of Geophysical Research, 117, B0248. http://dx.doi.org/10.1029/2011JB00882

Genser, J. and Neubauer, F., 1989. Low angle normal faults at the eastern margin of the Tauern Window (Eastern Alps). Mitteilungen der Österreichischen Geologischen Gesellschaft, 81, 233–243.

Genser, J., Van Wees, J.D., Cloething, S. and Neubauer, F., 1996. Eastern Alpine tectono-metamorphic evolution: constraints from two-dimensional PTt-modelling. Tectonics, 15, 584–604. http://dx.doi.org/10.1029/95TC03289

Gleadow, A.J.W., Hurford, A.J. and Quaife, R.D., 1976. Fission track dating of zircon: improved etching techniques. Earth and Planetary Science Letters, 33, 273–276. http://dx.doi.org/10.1016/0012-821X(76)90235-1

Gleadow, A.J.W., 1981. Fission-track dating methods: what are the real alternatives? Nuclear Tracks, 5, 3–14. http://dx.doi.org/10.1016/0191-278X(81)90021-4

Glotzbach, C., Reinecker, J., Danišík, M., Rahn, M., Frisch, W. and Spiegel, C., 2008. Neogene exhumation history of the Mont Blanc massif, Western Alps. Teconics. doi:10.1029/2007TC002247.

Grove, M. and Harrison, T., 1996. Ar diffusion in Fe-rich biotite. American Mineralogist, 81, 940–951.

Green, P.F., Duddy, I.R., Gleadow, A.J.W., Tingate, P.R. and Laslett, G.M., 1986. Thermal annealing of fission tracks in apatite 1. A qualitative description. Chemical Geology, 59, 237–253. http://dx.doi.org/10.1016/0168-9622(86)90074-6

Grundmann, G. and Morteani, G., 1985. The young uplift and thermal history of the central Eastern Alps (Austria, Italy), evidence from apatite fission track ages. Jahrbuch der Geologischen Bundesanstalt, Wien, 128, 197–216.

Guenthner, W. R., Reiners, P.W., Ketcham, R.A., Nasdala, L. and Giester, G., 2013. Helium diffusion in natural zircon: Radiation damage, anisotropy, and the interpretation of zircon (U-Th)/He thermochronology. American Journal of Science. 313(3), 145-198. http://dx.doi.org/10.2475/03.2013.01

Hames, W. and Bowering, S., 1994. An empirical evaluation of the argon diffusion geometry in muscovite. Earth and Planetary Science Letters, 124, 161–167. http://dx.doi.org/10.1016/0012-821X(94)00079-4

Handler, R., Dallmeyer, R.D. and Neubauer, F., 1997. $^{40}Ar/^{39}Ar$ ages of detrital white mica from Upper Austroalpine units in the Eastern Alps, Austria: Evidence for Cadomian and contrasting Variscan sources. Geologische Rundschau, 86, 69–80. http://dx.doi.org/10.1007/s005310050122

Harrison, T.M., Célérier, J., Aikman, A.B., Hermann, J. and Heizler, M.T., 2009. Diffusion of 40Ar in muscovite. Geochimica et Cosmochimica Acta, 73(4), 1029–1051. http://dx.doi.org/10.1016/j.gca.2008.09.038

Hejl, E., 1997. `Cold spots` during the Cenozoic evolution of the Eastern Alps: thermochronological interpretation of apatite fission-track data. Tectonophysics, 272, 159–173. http://dx.doi.org/10.1016/S0040-1951(96)00256-9

Hejl, E., 1998. Über die känozoische Abkühlung und Denudation der Zentralalpen östlich der Hohen Tauern – eine Apatit-Spaltspurenanalyse. Mitteilungen der Österreichischen Geologischen Gesellschaft, 89, 179–200.

Hoinkes, G., Höller, F., Rantitsch, G., Dachs, E., Höck, V., Neubauer, F., et al. 1999. Alpine metamorphism of the Eastern Alps. Schweizer Mineralogische und Petrographische Mitteilungen, 79, 155–181.

Hoke, L., 1990. The Altkristallin of the Kreuzeck Mountains, SE Tauern Window, Eastern Alps; basement crust in a convergent plate boundary zone. Jahrbuch der Geologischen Bundesanstalt, 133, 5–87.

Hopcroft, P., Gallagher, K., and Pain, C.C., 2007. Inference of past climate from borehole temperature data using Bayesian Reverse Jump Markov chain Monte Carlo. Geophysical Journal International, 171, 1430–1439. http://dx.doi.org/10.1111/j.1365-246X.2007.03596.x

Horvárth, F., Bada, G., Szafián, P., Tari, G., Ádám, A. and Cloething, S., 2006. Formation and deformation of the Pannonian Basin: constraints from observational data. In: D.G. Gee and R. Stephenson (eds.), European Lithosphere dynamics. Geological Society London Memoir, 32, pp. 191–206.

Hurford, J., and Green, P.F., 1983. The zeta age calibration of fission-track dating. Chemical Geology, 41, 285–312. http://dx.doi.org/10.1016/S0009-2541(83)80026-6

Jourdan, F. and Renne, P.R., 2007. Age calibration of the Fish Canyon sanidine $^{40}Ar/^{39}Ar$ dating standard using primary K–Ar standards. Geochimica et Cosmochimica Acta, 71, 387–402. http://dx.doi.org/10.1016/j.gca.2006.09.002

Ketcham, R.A., Donelick, R.A. and Carlson, W.D., 1999. Variability of apatite fission-track annealing kinetics III: Extrapolation to geological time scales. American Mineralogist, 84, 1235–1255.

Ketcham, R.A., Donelick, R.A. and Donelick, M.B., 2000. AFTSolve: a program for multi-kinetic modelling of apatite fission-track data. Mineralogical Society of America, 2, 1-32.

Ketcham, R.A., 2005. Forward and inverse modelling of low-temperature thermochronometry data. In: P. Reiners and T.A. Ehlers (eds.), Low-temperature thermochronology: techniques, interpretations and applications. Reviews in Mineralogy & Geochemistry, 58, 275–314.

Kirschner, D., Cosc, M., Masson, H. and Hunziker, J., 1996. Staircase 40Ar/39/Ar spectra of fine-grained white mica; timing and duration of deformation and empirical constraints on argon diffusion. Geology, 34(8), 747–750. http://dx.doi.org/10.1130/0091-7613(1996)024<0747:SAASOF>2.3.CO;2

Kralik, M., Klima, K. and Riedmüller, G., 1987. Dating fault gouges. Nature, 327, 315–317. http://dx.doi.org/10.1038/327315a0

Kurz, W. and Neubauer, F., 1996. Deformation partitioning during updoming of the Sonnblick area in the Tauern Window (Eastern Alps, Austria). Journal of Structural Geology, 18, 1327–1343. http://dx.doi.org/10.1016/S0191-8141(96)00057-0

Kurz, W. and Fritz, H., 2003. Tectonometamorphic evolution of the Austroalpine Nappe Complex in the central Eastern Alps – consequences for the Eo-alpine evolution of the Eastern Alps. International Geology Review, 45, 1100–1127. http://dx.doi.org/10.2747/0020-6814.45.12.1100

Kurz, W., Wölfler, A., Rabitsch, R. and Genser, J., 2011. Polyphase movement on the Lavanttal Fault Zone (Eastern Alps): reconciling the evidence from different geochronological indicators. Swiss Journal of Geosciences, 104(2), 323–343. http://dx.doi.org/10.1007/s00015-011-0068-y

Lambert, R.St.J., 1970. A potassium-argon study of the margin of the Tauernfenster at Döllach, Austria. Eclogae Geologicae Helvetiae, 63, 197–205.

Linner, M., Habler, G. and Grasemann, B., 2008. Vom Defereggen-Antholz-Vals-(DAV) zum Pustertal-Gailtal-Störungssystem: Mehrphasige spröde Deformation im Ostalpinen Kristallin. Journal of Alpine Geology, 49, 64–65.

Lips, A.L.W., White, S.H. and Wijbrans, J.R., 1998. $^{40}Ar/^{39}Ar$ laserprobe direct dating of discrete deformational events: a continuous record of early Alpine tectonics in the Pelagonian Zone, NE Aegean area, Greece. Tectonophysics, 298, 133–153. http://dx.doi.org/10.1016/S0040-1951(98)00181-4

Lippitsch, R., Kissling, E. and Ansorge, J., 2003. Upper mantle structure beneath the Alpine orogen from high-resolution teleseismic tomography. Journal of Geophysical Research, 108, B8, 2376. http://dx.doi.org/10.1029/2002JB002016

Liu, Y., Genser, J., Handler, R., Friedl, G. and Neubauer, F., 2001. $^{40}Ar/^{39}Ar$ muscovite ages from the Penninic-Austroalpine plate boundary, Eastern Alps. Tectonics, 20, 526–547. http://dx.doi.org/10.1029/2001TC900011

Luth, S.W. and Willingshofer, E., 2008. Mapping of the post-collisional cooling history of the Eastern Alps. Swiss Journal of Geosciences, 101(1), 207–223. http://dx.doi.org/10.1007/s00015-008-1294-9

Mancktelow, N.S., Stöckli, D.F., Grollimund, B., Müller, W., Fügenschuh, B., Viola, G., Seward, D. and Villa, I.M., 2001. The DAV and Periadriatic fault systems in the Eastern Alps south of the Tauern Window. International Journal of Earth Sciences, 90, 593–622. http://dx.doi.org/10.1007/s005310000190

Meesters, A.G.C.A. and Dunai, T.J., 2002. Solving the production–diffusion equation for finite diffusion domains of various shapes part 2, Application to cases with Alpha ejection and non-homogeneous distribution of the source. Chemical Geology, 186(3–4), 345–363. http://dx.doi.org/10.1016/S0009-2541(02)00072-4

Most, P., 2003. Late Alpine cooling histories of tectonic blocks along the central part of the TRANSALP-traverse (Inntal-Gardertal): constraints from geochronology. Tübinger Geowissenschaftliche Arbeiten, Reihe A 67, 97 pp.

Müller, D., Stumpfl, E.F. and Taylor, W.R., 1992. Soshonitic and alkaline lamprophyres with elevated Au and PGE concentrations from the Kreuzeck Mountains, Eastern Alps, Austria. Contributions to Mineralogy and Petrology, 46, 23–42. http://dx.doi.org/10.1007/BF01160699

Müller, W., Mancktelow, N.S. and Meier, N., 2000. Rb-Sr microchrons of synkinematic mica in mylonites: an example from the DAV fault of the Eastern Alps. Earth and Planetary Science Letters, 180, 385–397. http://dx.doi.org/10.1016/S0012-821X(00)00167-9

Neubauer, F. and Handler, R., 2000. Variscan orogeny in the Eastern Alps and Bohemian Massif: How do these units correlate? Mitteilungen der Österreichischen Geologischen Gesellschaft, 92, 35–59.

Neubauer, F., Dallmeyer, R.D., Dunkl, I. and Schimik, D., 1995. Late Cretaceous exhumation of the metamorphic Gleinalm dome, Eastern Alps: Kinematics, cooling history and sedimentary response in a sinistral wrench corridor. Tectonophysics, 242, 79–98. http://dx.doi.org/10.1016/0040-1951(94)00154-2

Neubauer F., Hoinkes, G., Sassi, F.P., Handler, R., Höck, V., Koller, F., et al. 1999. Pre-Alpine metamorphism of the Eastern Alps. Schweizer Mineralogische und Petrographische Mitteilungen, 79, 41–62.

Neubauer, F., Genser, J. and Handler, R., 2000. The Eastern Alps: Result of a two-stage collision process. Mitteilungen der Österreichischen Geologischen Gesellschaft, 92, 117–134.

Ortner, H., 2007. Styles of soft-sediment deformation on top of a growing fold system in the Gosau at Muttekopf, Northern Calcareous Alps, Austria: Slumping versus tectonic deformation. Sedimentary Geology, 196, 99–118. http://dx.doi.org/10.1016/j.sedgeo.2006.05.028

Oxburgh, E.R., Lambert, R.St.J., Baadsgaard, H. and Simons, J.G., 1966. Potassium-argon age studies across the southeastern margin of the Tauern Window, the Eastern Alps. Verhandlungen der Geologischen Bundesanst Wien, 17–33.

Polinski, R.K. and Eisbacher, G.H., 1992. Deformation partitioning during polyphase oblique convergence in the Karawanken Mountains, southeastern Alps. Journal of Structural Geology, 14, 1203-1213. http://dx.doi.org/10.1016/0191–8141(92)90070-D

Pomella, H., Klötzli, U., Scholger, R., Stipp, M. and Fügenschuh, B., 2010. The northern Guidicarie and the Meran – Mauls fault (Alps, northern Italy) in the light of new paleomagnetic and geochronological data from boudinaged Eo-/Oligocene tonalities. International Journal of Earth Sciences. http://dx.doi.org/10.1007/s00531-010-0612-4

Rantitsch, F., 2000. Die Wärmegeschichte des Drauzuges (Ostalpen). Mitteilungen der Gesellschaft der Geologie und Bergbaustudenten in Österreich, 43, 110–111.

Ratschbacher, L., Merle, O., Davy, P. and Cobbold, P., 1991a. Lateral extrusion in the Eastern Alps: Part 1. Boundary conditions and experiments scaled for gravity. Tectonics, 10, 245–256. http:/dx.doi.org/10.1029/90TC02622

Ratschbacher, L., Frisch, W., Linzer, H.G. and Merle, O., 1991b. Lateral extrusion in the Eastern Alps: Part 2. Structural analysis. Tectonics, 10, 257–271. http://dx.doi.org/10.1029/90TC02623

Reiners, P.W., Zhou, Z., Ehlers, T.A., Xu, C., Brandon, M.T., Donelick, R.A. and Nicolescu, S., 2003. Post-orogenic evolution of the Dabie Shan, Eastern China, from (U-Th)/He and fission track thermochronology. American Journal of Science, 303, 489–518. http://dx.doi.org/10.2475/ajs.303.6.489

Reiners, P.W., Spell, T.L., Nicolescu, S. and Zanetti, K.A., 2004. Zircon (U-Th)/He thermochronometry: He diffusion and comparisons with 40Ar/39Ar dating. Geochimica et Cosmochimica Acta, 68(8), 1857-1887. http://dx.doi.org/10.1016/j.gca.2003.10.021

Renne, P.R., Deino, A.L., Walter, R.C., Turrin, B.D., Swisher, C.C., Becker, G.H., Curtis, W.D., Sharo, W.D. and Jaouni, A. R., 1994. Intercalibration of astronomical and radioisotopic time. Geology, 22, 783–786. http://dx.doi.org/10.1130/0091-7613(1994)022<0783:IOAART>2.3.CO;2

Sachsenhofer, R.F., 2001. Syn- and postcollisional heat flow in the Cenozoic Eastern Alps. International Journal of Earth Sciences, 90, 579–592. http://dx.doi.org/10.1007/s005310000179

Sambridge, M., Gallagher, K., Jackson, A. and Rickwood, P., 2006. Transdimensional inverse problems, Model Comparison and the Evidence. Geophysical Journal International, 167, 528–542. http://dx.doi.org/10.1111/j.1365-246X.2006.03155.x

Scharf, A., Handy, M.R., Favaro, S., Schmid, S.M. and Bertrand, A., 2013. Modes of orogen-parallel stretching and extensional exhumation in response to microplate indentation and roll-back subduction (Tauern Window, Eastern Alps). International Journal Earth of Earth Sciences. http://dx.doi.org/10.1007/s00531-013-0894-4

Schmid, S.M., Fügenschuh, B., Kissling, E. and Schuster, R., 2004. Tectonic map and overall architecture of the Alpine orogen. Eclogae Geologicae Helveticae, 97, 93-117. http://dx.doi.org/10.1007/s00015-004-1113-x

Schmid, S.M., Scharf, A., Handy, M.R. and Rosenberg, C.L., 2013. The Tauern Window (Eastern Alps, Austria): a new tectonic map, with cross-sections and a tectonometamorphic synthesis. Swiss Journal of Geosciences, 106, 1–32. http://dx.doi.org/10.1007/s00015-013-0123-y

Schuster, R. and Stüwe, K., 2008. Permian metamorphic event in the Alps. Geology, 36, 603-606. http://dx.doi.org/10.1130/G24703A.1

Schuster, R., Scharbert, S., Abart, R. and Frank, W., 2001. Permo-Triassic extension and related HT/LP metamorphism in the Austroalpine – Southalpine realm. Mitteilungen der Gesellschaft der Geologie und Bergbaustudenten in Österreich, 45, 111–141.

Schuster, R., Koller, F., Hoeck, V., Hoinkes, G. and Bousquet, R., 2004. Explanatory notes to the map: metamorphic structure of the Alps - Metamorphic evolution of the Eastern Alps. Mitteilungen der Österreichischen Mineralogischen Gesellschaft, 149, 175–199.

Schuster, R., Kurz, W., Krenn, K. and Fritz, H., 2013. Introduction to the Geology of the Eastern Alps. Berichte der Geologischen Bundesanstalt, Wien, 99, 121–133.

Selverstone, J., 1988. Evidence for east-west crustal extension in the Eastern Alps: implications for the unroofing history of the Tauern Window. Tectonics, 7, 87–105. http://dx.doi.org/10.1029/TC007i001p00087

Sölva, H., Grasemann, B., Thöni, M., Thiede, R.C. and Habler, G., 2005. The Schneeberg Normal Fault Zone: Normal faulting associated with Cretaceous SE-directed extrusion in the Eastern Alps (Italy/Austria). Tectonophysics, 401, 143–166. http://dx.doi.org/10.1016/j.tecto.2005.02.005

Staufenberg, H., 1987. Apatite fission-track evidence for postmetamorphic uplift and cooling history of the eastern Tauern Window and the surrounding Austroalpine (Central Eastern Alps, Austria). Jahrbuch der Geologischen Bundesanstalt, 13, 571–586.

Steenken, A., Siegesmund, S., Heinrich, T. and Fügenschuh, B., 2002. Cooling and exhumation of the Rieserferner Pluton (Eastern Alps, Italy/Austria). International Journal of Earth Sciences, 91, 799–817. http://dx.doi.org/10.1007/s00531-002-0260-4

Steiger, R.H. and Jäger, E., 1977. Subcommission on Geochronology: convention on the use of decay constants on Geo- and Cosmochronology. Earth and Planetary Science Letters, 36, 359–362. http://dx.doi.org/10.1016/0012-821X(77)90060-7

Stephenson, J., Gallagher, K. and Holmes, C., 2006. Low temperature thermochronology and modelling strategies for multiple samples 2: Partition modelling for 2D and 3D distributions with discontinuities. Earth and Planetary Science Letters, 241, 557–570. http://dx.doi.org/10.1016/j.epsl.2005.11.027

Stöckhert, B., Brix, M.R., Kleinschrodt, R., Hurford, A.J. and Wirth, R., 1999. Thermochronometry and microstructures of quartz – a comparison with experimental flow laws and predictions on the temperature of brittle-plastic transition. Journal of Structural Geology, 21, 351–369. http://dx.doi.org/10.1016/S0191-8141(98)00114-X

Stüwe, K., White, L. and Brown, R., 1998. The influence of eroding topography on steady-state isotherms. Application to fission track analysis. Earth and Planetary Science Letters, 124, 63–74. http://dx.doi.org/10.1016/0012-821X(94)00068-9

Stüwe, K. and Hintermüller, M., 2000. Topography and isotherms revisited: the influence of laterally migrating drainage divides. Earth and Planetary Science Letters, 184, 287–303. http://dx.doi.org/10.1016/S0012-821X(00)00315-0

Thöni, M., 1999. A review of geochronological data from the Eastern Alps. Schweizer Mineralogische und Petrographische Mittleilungen, 79, 281–303.

Thöni, M., 2006. Dating eclogite-facies metamorphism in the Eastern Alps – approaches, results, interpretations: a review. Mineralogy and Petrology, 88, 123–148. http://dx.doi.org/10.1007/s00710-006-0153-5

Villa, I.M., 1998. Isotopic closure. Terra Nova, 10, 42–47.

Viola, G., Mancktelow, N.S. and Seward, D., 2001. Late Oligocene-Neogene evolution of Europe-Adria collision: new structural and geochronological evidence from the Giudicarie fault system (Italy, Eastern Alps). Tectonics, 20, 999–1020. http://dx.doi.org/10.1029/2001TC900021

Wagner, G.A., 1968. Fission track dating of apatites. Earth and Planetary Science Letters, 4, 411–415. http://dx.doi.org/10.1016/0012-821X(68)90072-1

Wagner, G.A. and Reimer, G.M., 1972. Fission track tectonics: the tectonic interpretation of fission track apatite ages. Earth and Planetary Science Letters, 14, 263–268. http://dx.doi.org/10.1016/0012-821X(72)90018-0

Wagner, G.A., Reimer, G.M. and Jäger, E., 1977. Cooling ages derived by Apatite Fission-Track, Mica Rb-Sr and K-Ar dating: The uplift and cooling history of the Central Alps. Memorie degli Istituti di Geologia e Mineralogia dellÚniversitá di Padova, 30, 27 pp.

Wagner, G.A, and van den Haute P., 1992. Fission-Track Dating. Enke, Stuttgart, 285 pp.

Wagreich, M. 1995. Subduction tectonic erosion and Late Cretaceous subsidence along the northern Austroalpine margin (eastern Alps, Austria). Tectonophysics, 242, 63-78. http://dx.doi.org/10.1016/0040-1951(94)00151-X

Watson, E.B. and Harrison, T.M., 1983. Zircon saturation revisited; temperature and composition effects in a variety of crustal magma types. Earth and Planetary Science Letters, 64(2), 295–304. http://dx.doi.org/10.1016/0012-821X(83)9021 1-X

Wendt, A.S., Vidal, O. and Chadderton, L.T., 2002. Experimental evidence for the pressure dependence of fission track annealing in apatite; intimidating implications? Earth and Planetary Science Letters, 201, 593–607. http://dx.doi.org/10.1016/S0012-821X(02)00727-6

Wölfler, A., Dekant, C., Danišík, M., Kurz, W., Dunkl, I., Putiš, M. and Frisch, W., 2008. Late stage differential exhumation of crustal blocks in the central Eastern Alps: evidence from fission track and (U-Th)/He thermochronology. Terra Nova, 20, 378–384. http://dx.doi.org/10.1111/j.1365-3121.2008.00831.x

Wölfler, A., Kurz, W., Danišík, M. and Rabitsch, R., 2010. Dating of fault zone activity by apatite fission track and apatite (U-Th)/He thermochronometry: a case study from the Lavanttal fault system (Eastern Alps). Terra Nova, 22, 274–282. http://dx.doi.org/10.1111/j.1365-3121.2010.00943.x

Wölfler, A., Kurz, W., Fritz, H. and Stüwe, K., 2011. Lateral extrusion in the Eastern Alps revisited: refining the model by thermochronological, sedimentary and seismic data. Tectonics, 30, TC4006. http://dx.doi.org/10.1029/2010TC002782

Wölfler, A., Stüwe, K., Danišík, M. and Evans, N.J., 2012. Low temperature thermochronology in the Eastern Alps: Implications for structural and topographic evolution. Tectonophysics. http://dx.doi.org/10.1016/j.tecto.2012.03016

Received: 24 March 2014
Accepted: 23 September 2014

Andreas WÖLFLER[1)*)], Christian DEKANT[2)], Wolfgang FRISCH[2)], Martin DANIŠÍK[3)] & Wolfgang FRANK[4)]

[1)] Institut für Geologie, Leibniz Universität Hannover, Callinstraße 30, D-30167 Hannover, Germany;

[2)] Institut für Geowissenschaften, Wilhelmstraße 56, D-72074 Tübingen, Germany;

[3)] Department of Earth & Ocean Sciences, Faculty of Science & Engineering, The University of Waikato, Hillcrest Road, Hamilton 3240, New Zealand;

[4)] Geological Institute, Slovak Academy of Sciences, Dúbravská cesta 9, SK-84005, Bratislava 45, Slovak Republic;

[*)] Corresponding author, woelfler@geowi.uni-hannover.de